

---

# FROM PIXELS TO PARCELS: FLEXIBLE, PRACTICAL SMALL-AREA UNCERTAINTY ESTIMATION FOR SPATIAL AVERAGES OBTAINED FROM ABOVEGROUND BIOMASS MAPS

---

A PREPRINT

**Lucas K Johnson** 

Department of Sustainable Resources Management  
State University of New York College of Environmental Science and Forestry  
Syracuse, NY, 13210  
[johnsl27@oregonstate.edu](mailto:johnsl27@oregonstate.edu)

**Grant M Domke** 

Northern Research Station  
USDA Forest Service  
St. Paul, MN, 55114  
[grant.m.domke@usda.gov](mailto:grant.m.domke@usda.gov)

**Stephen V Stehman** 

Department of Sustainable Resources Management  
State University of New York College of Environmental Science and Forestry  
Syracuse, NY, 13210  
[svstehma@esf.edu](mailto:svstehma@esf.edu)

**Michael J Mahoney** 

Department of Sustainable Resources Management  
State University of New York College of Environmental Science and Forestry  
Syracuse, NY, 13210  
[mjmahone@esf.edu](mailto:mjmahone@esf.edu)

**Colin M Beier** 

Department of Sustainable Resources Management  
State University of New York College of Environmental Science and Forestry  
Syracuse, NY, 13210  
[cbeier@esf.edu](mailto:cbeier@esf.edu)

2024-12-20

## ABSTRACT

Fine-resolution maps of forest carbon and aboveground biomass (AGB) effectively represent spatial patterns and can be flexibly aggregated to map subregions by computing spatial averages or totals of pixel-level predictions. However, generalized model-based uncertainty estimation for spatial aggregates requires computationally expensive processes like iterative bootstrapping and computing pixel covariances. Uncertainty estimation for map subregions is critical for enhancing practicality and eventual adoption of model-based data products, as this capability would empower users to produce estimates at scales most germane to management of the landscape: individual forest stands

and ownership parcels. In this study we produced estimates of standard error (SE) associated with spatial averages of fine-resolution AGB map predictions for a stratified random sample of ownership parcels (0-5000 acres) in New York State (NYS). This represents the first model-based uncertainty estimation study to include all four types of uncertainty (reference data, sample variability, residual variability, and auxiliary data), incorporate spatial autocorrelation of model residuals, and use methods compatible with algorithmic modeling (machine learning or nonparametric). We found that uncertainty attributed to residual variance, largely resulting from spatial correlation of residuals, dominated all other sources for the majority of the parcels in the study (0-2500 acres). These results suggest that improvements to model accuracy will yield the greatest reductions to total uncertainty in regions like the northeastern and midwestern United States where forests are divided into smaller spatial units. Further, we demonstrated that log-log regression relating parcel characteristics (area, perimeter, AGB density, forest cover) to parcel-level SE can accurately estimate uncertainty for map subregions, thus providing a convenient means to empower map users. These findings support transparency in future regional-scale model-based forest carbon accounting and monitoring efforts.

**Keywords** model-based inference • bootstrap • Landsat • machine learning • national forest inventory • Forest Inventory and Analysis

## 1 Introduction

Over the past 30 years, greenhouse gas (GHG) accounting efforts have proliferated from local to global scales and across private and public sectors. These efforts began in 1992 with the United Nations requiring all developed countries to report annual emissions (“The United Nations Framework Convention on Climate Change” 1992), and since have evolved into the Kyoto Protocol (“Kyoto Protocol to the United Nations Framework Convention on Climate Change” 1997), and the Paris Climate agreement (“Paris Agreement to the United Nations Framework Convention on Climate Change” 2015) with accounting methodologies and practices defined by the 2019 IPCC update on GHG inventory methods (Buendia et al. 2019). These standards require that GHG emissions and removals be reported with confidence intervals and with uncertainties reduced as far as possible (Penman et al. 2003; Eggleston et al. 2006). Beyond satisfying these requirements, identifying and understanding sources of uncertainty are critical for distinguishing between noise and real GHG emissions and removals. Forests are among the most effective carbon sinks with global net sequestration rates estimated at 1.1 (+/- 0.8) Pg of carbon per year (Pan et al. 2011). However, the strength of this sink is not spatially consistent and in some regions forest lands may be net carbon sources due to deforestation and degradation (Pan et al. 2011). Consequently, a significant body of research is dedicated to accounting for forest carbon fluxes with improved accuracy, precision, and spatial resolution.

Many large-scale forest carbon accounting approaches leverage the extensive sampling designs of national forest inventories (NFI) to estimate annual emissions and removals from the forest sector (Woodall et al. 2015; McRoberts, Tomppo, and Næsset 2010). These design-based estimators are often accompanied by relatively accessible estimators of variance, which account for sampling variability but omit variability related to tree- and plot-level predictions (reference data uncertainty) since population units are assumed to have a single fixed value under the design-based framework (McRoberts 2011; McRoberts et al. 2022). Although design-based approaches offer fundamental insights and essential data on forest carbon dynamics, they are often limited spatially and temporally by sampling density and measurement frequency respectively (McRoberts 2011), and thus cannot represent fine-scale patterns and dynamics most relevant to planning and decision-making. Model-based approaches, which combine field data (e.g. NFI plots) with wall-to-wall, remotely-sensed data can fill this need by producing predictions for all map units (pixels) in a given area (Kennedy, Ohmann, et al. 2018; Matasci et al. 2018; Huang et al. 2019; Hudak et al. 2020; L. K. Johnson et al. 2022, 2023).

Although model-based approaches offer enhanced spatial flexibility relative to their design-based counterparts, they rely on different assumptions and require a more complex combination of terms for estimating uncertainty. Under model-based inferential frameworks, variability is derived from the assumption that each population unit has an entire distribution of possible values, with each random realization of a population unit value corresponding to a single distinct population from an overarching set of populations known as a super-population (McRoberts et al. 2022). Following model-based terminology, super-population parameters are thus estimated, whereas population parameters are predicted (McRoberts et al. 2022). Model-based estimates of uncertainty may include the following components: uncertainty in reference data (Table 1, type a), uncertainty due to training the model on a sample (Table 1, type b), uncertainty due to the model not being able to represent all of the variation in the response variable (Table 1, type c), and auxiliary data uncertainty (Table 1, type d) (Wadoux and Heuvelink 2023; CEOS 2021). Different terms have been used to refer to type b, including model parameter/prediction covariance, model parameter/prediction uncertainty (McRoberts et al. 2018), or sampling variability (CEOS 2021; McRoberts et al. 2022) since model parameter estimates and subsequent predictions depend on the training data sample. Type c is usually called residual variability and is sometimes broken down into components quantifying residual variance and spatial covariance of residuals (McRoberts et al. 2018, 2022;

CEOS 2021). The proportion of model-based studies that produce uncertainty estimates is small (McRoberts 2011), likely because the technical complexity of generating uncertainty estimates is substantially greater than that of making predictions.

From the model-based studies that do include estimates of uncertainty, desirable features for the uncertainty estimation process include:

1. Flexibility to incorporate parametric as well as algorithmic models (i.e. machine learning and nonparametric models).
2. Incorporating all four types of uncertainty (Table 1).
3. Methods for producing uncertainty estimates for spatial averages or totals that explicitly account for spatial autocorrelation of residuals.
4. Consideration of computational efficiency and delivery to map users.

Applications of rigorous model-based uncertainty estimation have been advanced using parametric models with accompanying analytic estimators of variance (Saarela et al. 2020, 2018, 2016; Chen et al. 2016; Chen, Laurin, and Valentini 2015; McRoberts et al. 2018). However, these analytic estimators are fairly complex, and can be inaccessible for practitioners lacking deep backgrounds in statistics or mathematics. Further, requiring parametric models may be limiting, and thus in violation of desirable criterion 1 (defined above), as algorithmic approaches may yield improved predictive accuracy (Efron 2020; Breiman 2001b). At the cost of computational efficiency, iterative approaches like bootstrapping or Monte Carlo simulations, however, are flexible to model form, can easily incorporate uncertainty from several sources, and are conceptually simple relative to analytic estimators (McRoberts et al. 2022; CEOS 2021; Esteban et al. 2020).

Reference data uncertainty (Table 1, type a) is often deemed negligible or is omitted due to a scarcity of representative data describing measurement error and allometric uncertainty (Breidenbach et al. 2014), thus violating desirable criterion 2 (defined above). For forest aboveground biomass (AGB) or carbon studies in particular, reference data may be highly uncertain, given that tree-level AGB values in NFIs are typically predictions themselves. Instead, tree-level biomass and carbon are modeled as a function of measured variables like diameter and height using allometric models developed for particular regions and taxa (Jenkins et al. 2003; Woodall et al. 2011; Chave et al. 2014). The measured variables themselves are subject to error and imprecision, further contributing to the overall uncertainty of the tree-level predictions (Berger et al. 2014; Yanai et al. 2023). It is largely agreed that tree-level uncertainty contributes a small fraction of the total uncertainty when aggregated over many individuals for design-based estimates at coarse scales (Breidenbach et al. 2014; Ståhl et al. 2014; McRoberts and Westfall 2014; Yanai et al. 2023), yet whether or not these small fractions can be considered negligible across scales and contexts is unresolved (Chen, Laurin, and Valentini 2015; McRoberts et al. 2016; Saarela et al. 2020). Considering the range of reference data uncertainty contributions reported in the model-based estimation literature (5% of pixel-level uncertainty Chen, Laurin, and Valentini (2015); 75% of 5005 km<sup>2</sup> area uncertainty Saarela et al. (2020)), it remains prudent to include this component to the extent that it is feasible.

Model-based estimates of pixel- or point-level uncertainty (i.e. uncertainty maps), though helpful to identify the spatial distribution of uncertainties within an area, should be accompanied with methods to aggregate uncertainties to produce estimates at scales relevant to management and decision making like individual forest stands and ownership parcels (desirable criterion 3, defined above). Spatially aggregating predictions can be achieved by averaging or summing all predictions within a given area. However, spatially aggregating uncertainties requires data beyond that which is contained in an uncertainty map (Wadoux and Heuvelink 2023; McRoberts et al. 2022). Specifically, pairwise prediction or residual covariances and associated spatial correlations are required but do not fit into an uncertainty map ( $N^2$  pairs but  $N$  map pixels) and may present obstacles. First, computing the necessary prediction or residual covariances for a given area is often computationally expensive; second, obtaining the spatially dense reference data (i.e. short distances between plots) needed to incorporate spatial autocorrelation of residuals is often prohibitive (Breidenbach, McRoberts, and Astrup 2016; McRoberts et al. 2022; Wadoux and Heuvelink 2023). If estimates are only to be produced for large units of aggregation (e.g. polygons with dimensions well beyond the range of spatial autocorrelation) then the contribution from spatially autocorrelated residuals is negligible, however, for scales germane to forest management (i.e. stands and parcels) this component may be highly relevant (Breidenbach, McRoberts, and Astrup 2016; McRoberts et al. 2018, 2022).

McRoberts et al. (2022) considered the feasibility of efficiently producing uncertainty estimates for map subregions, both internally as a map producer but also for map users in satisfaction of desirable criterion 4 (defined above). Their approach was predicated on methods for reducing the size of the metadata needed to estimate uncertainty for map subregions to transfer this metadata more easily to users. However, McRoberts et al. (2022) applied their proposed approach only to relatively large areas (2500 km<sup>2</sup> and 12,500 km<sup>2</sup>) for which the effects of spatial autocorrelation

Table 1: Categorization of four types of model-based uncertainty considered in this study, and how they contribute (variance component) to the estimates of total variance ( $\text{Var}_{\text{total}}$ ).

Type	Name	Source of Uncertainty	Variance Component
a	Reference data uncertainty ( $\text{Var}_{\text{ref}}$ )	Measurement, classification, allometric model, and plot location errors	$\text{Var}_{\text{boot}}$
b	Sampling variability ( $\text{Var}_{\text{sam}}$ )	Training the model on a sample	$\text{Var}_{\text{boot}}$
c	Residual variability	The model is not able to represent all variation in the response variable	$\text{Var}_{\text{res}}$
d	Auxiliary data uncertainty ( $\text{Var}_{\text{LC}}$ )	Variability related to sensor imprecision and inaccuracy or model uncertainty if the data are model generated	$\text{Var}_{\text{boot}}$

of residuals could be ignored. Further, this approach requires a sophisticated series of operations including the reclassification of pixel-predictions into bins, a lookup of bin covariances in a provided matrix for each pixel pair, and summation of covariances for all pixel pairs in the region of interest.

In this study we built on the methods developed in McRoberts et al. (2022) to produce model-based estimates of uncertainty (standard error; SE) associated with spatial averages of AGB predictions for small ownership parcels (spatial units of analysis sized <1-5000 acres) in New York State (NYS). We replicated the machine learning modeling framework developed in L. K. Johnson et al. (2023) to produce pixel-level AGB predictions. We had three objectives: 1) to estimate a model-based SE that included all four types of uncertainty (Table 1, types a-d), incorporated spatial autocorrelation of model residuals, and used methods that are compatible with algorithmic modeling; 2) estimate the relative contributions of uncertainty components across scales to help direct further efforts toward reducing total uncertainties in model-based estimates; and 3) derive a relationship between ownership parcel characteristics (area, perimeter, AGB density, % forest cover) and SE in the form of a multiple regression model to provide a practical, broadly applicable method for uncertainty estimation for map subregions that both map users and producers can implement, satisfying desirable criterion 4.

## 2 Data and Methods

### 2.1 Overview

We largely followed the steps described in McRoberts et al. (2022) to produce estimates of total variance and standard error (SE) associated with spatial averages of aboveground biomass (AGB) predictions for a stratified random sample of small ownership parcels (<1-5000 acres) in New York State (NYS; Figure 1). Pixel-level AGB predictions were made with a machine learning ensemble model developed in L. K. Johnson et al. (2023) (“direct” approach) which relied on Landsat imagery and was trained on plot-level AGB predictions from the United States Forest Inventory and Analysis (FIA) program (Bechtold and Patterson 2005; Gray et al. 2012). The total variance for a given parcel was estimated as the sum of two components, and the SE was computed as the square root of total variance as follows:

$$\text{Var}_{\text{total}} = \text{Var}_{\text{boot}} + \text{Var}_{\text{res}} \quad (1)$$

$$\text{SE} = \sqrt{\text{Var}_{\text{total}}} \quad (2)$$

Implicit in these formulas is the assumption that components  $\text{Var}_{\text{boot}}$  are  $\text{Var}_{\text{res}}$  are independent, but interrogating this assumption was beyond the scope of this study.

After computing  $\text{Var}_{\text{total}}$  and SE for each parcel in our sample, we further deconstructed the  $\text{Var}_{\text{boot}}$  component and evaluated the relative contributions of each sub-component to the total. Further, we fit a regression model to estimate SE for a given parcel as a function of the following parcel characteristics: area, perimeter, AGB, and forest cover. This regression model was developed to expedite the process of uncertainty estimation for any specified subregion of interest. All data compilation, modeling, analysis, and summary were conducted using the R programming language (R Core Team 2023) with the targets pipeline tool (Landau 2021).

## 2.2 Bootstrap variance

This component includes uncertainty in reference data (Table 1, type a), uncertainty due to training a model on a sample (Table 1, type b), and uncertainty related to the landcover mask used in our areal estimates (Table 1, type d). The same iterative bootstrapping approach was used to include each of these three types of uncertainty. Specifically, in each iteration  $i$  of 1000 iterations, a new training data set was developed as follows (additional details for some steps are provided in the subsections noted in parentheses):

1. A sample was selected with replacement from the original sample of FIA field plots.
2. New tree-level AGB predictions were produced for all trees in the new sample of plots. Residuals were drawn from both empirical and estimated distributions to account for measurement error and allometric uncertainty/error in tree-level biomass predictions (Section 2.5.1; Section 2.5.2).
3. These new tree-level AGB predictions were aggregated within each plot to produce plot-level AGB in units of megagrams per hectare  $\text{Mg ha}^{-1}$ .
4. A residual was randomly selected from an estimated distribution of plot-location errors yielding a new plot geometry from which auxiliary data were extracted (Section 2.5.3; Section 2.6).

Next, machine learning (ML) ensembles were fit to each training data set  $i$ , and then used to make a set of predictions for the map units (pixels) within each parcel, resulting in 1000 predictions per pixel (Section 2.7). The bootstrap variance for a given parcel was then computed as the variance over 1000 replications of the parcel-level AGB density, where AGB density was computed as the average of all pixel-predictions within the parcel. Specifically, the bootstrap variance was computed with the following equation:

$$\text{Var}_{\text{boot}} = \frac{\sum_{i=1}^n (\hat{u}_i - \hat{u})^2}{n - 1} \quad (3)$$

where  $n$  is the number of bootstrap iterations,  $\hat{u}$  is the average parcel-level AGB density over  $n$  iterations, and  $\hat{u}_i$  is the parcel-level AGB density estimated for a given bootstrap iteration  $i$  and computed as:

$$\hat{u}_i = \frac{\sum_{i=1}^N \hat{y}_i}{N} \quad (4)$$

where  $N$  is the number of pixels in a given parcel and  $\hat{y}_i$  is a pixel-level AGB prediction made by the ML ensemble. Derivations for and examples of these bootstrap procedures and equations can be found in Freedman (1981), Efron and Tibshirani (1994), CEOS (2021), and McRoberts et al. (2022).

To better understand the relative contributions of various sources of uncertainty, we further deconstructed  $\text{Var}_{\text{boot}}$  into reference data variance ( $\text{Var}_{\text{ref}}$ ; Table 1, type a), sample variance ( $\text{Var}_{\text{sam}}$ ; Table 1, type b), and landcover mask variance ( $\text{Var}_{\text{LC}}$ ; Table 1, type d) such that:

$$\text{Var}_{\text{boot}} = \text{Var}_{\text{ref}} + \text{Var}_{\text{sam}} + \text{Var}_{\text{LC}} \quad (5)$$

Each respective sub-component was computed by subtraction. To compute  $\text{Var}_{\text{sam}}$ , a 1000 iteration simulation was run with a constant training data set across each iteration. The resulting estimate of  $\text{Var}_{\text{boot}}$ , identified here as  $\text{Var}_{\text{boot-no-resample}}$ , was then subtracted from the original estimate of  $\text{Var}_{\text{boot}}$  to produce  $\text{Var}_{\text{sam}}$  as follows:

$$\text{Var}_{\text{sam}} = \text{Var}_{\text{boot}} - \text{Var}_{\text{boot-no-resample}} \quad (6)$$

Similarly, to compute  $\text{Var}_{\text{LC}}$ , a 1000 iteration simulation was run with a constant landcover mask (Section 2.7) across each iteration. The resulting estimate of  $\text{Var}_{\text{boot}}$ , identified here as  $\text{Var}_{\text{boot-static-LC}}$ , was then subtracted from the original estimate of  $\text{Var}_{\text{boot}}$  to produce  $\text{Var}_{\text{LC}}$  as follows:

$$\text{Var}_{\text{LC}} = \text{Var}_{\text{boot}} - \text{Var}_{\text{boot-static-LC}} \quad (7)$$

In cases where the sum of  $\text{Var}_{\text{sam}}$  and  $\text{Var}_{\text{LC}}$  was greater than  $\text{Var}_{\text{boot}}$ , the difference between  $\text{Var}_{\text{boot}}$  and the sum of  $\text{Var}_{\text{sam}}$  and  $\text{Var}_{\text{LC}}$  was proportionally subtracted from each variance component ( $\text{Var}_{\text{sam}}$ ,  $\text{Var}_{\text{LC}}$ ). Finally, estimates of  $\text{Var}_{\text{sam}}$  and  $\text{Var}_{\text{LC}}$  were subtracted from original estimates of  $\text{Var}_{\text{boot}}$  to produce  $\text{Var}_{\text{ref}}$  as follows:

$$\text{Var}_{\text{ref}} = \text{Var}_{\text{boot}} - \text{Var}_{\text{sam}} - \text{Var}_{\text{LC}} \quad (8)$$

### 2.3 Residual variance

This component contributes to uncertainty due to the model failing to represent all of the variation in the response variable (Table 1, type c). Because model residuals had non-constant variance, we fit a model to estimate residual variance as a function of our AGB predictions (Section 2.8). We used this model to make pixel-level residual variance estimates that aligned with individual AGB predictions. We then aggregated pixel-level residual variance to each parcel as follows:

$$\text{Var}_{\text{res}} = \frac{\sum_{i=1}^N \hat{\sigma}_i^2}{N^2} + \frac{\sum_{i=1, i \neq j}^N \sum_{j=1}^N \hat{\sigma}_i \hat{\sigma}_j \hat{\rho}_{ij}}{N^2} \quad (9)$$

where  $\hat{\sigma}_i^2$  is the estimated residual variance for a given pixel,  $N$  is the number of pixels in a given parcel, and  $\hat{\rho}_{ij}$  is the estimate of spatial correlation between pixel-level residuals defined as

$$\hat{\rho}_{ij} = \frac{\text{sill} - \gamma(h)}{\text{sill}} \quad (10)$$

where  $\gamma$  is a semivariogram function,  $h$  is the distance between pixels  $i$  and  $j$ , and  $\text{sill}$  is the semivariance ceiling estimated from the semivariogram. Derivations for Equation 9 can be found in McRoberts et al. (2022), and derivations for Equation 10 can be found in Wadoux and Heuvelink (2023) and Webster and Oliver (2007).

The semivariogram function used in Equation 10 (further described in Section 2.9) was fit to a simple random sample of spatial residuals (pixels) computed as follows:

$$\hat{e}_i = \hat{y}_{i-\text{Landsat}} - \hat{y}_{i-\text{LiDAR}} \quad (11)$$

where  $\hat{y}_{i-\text{Landsat}}$  is an AGB prediction from the Landsat-based model evaluated in this study (Section 2.7; L. K. Johnson et al. (2023)), and  $\hat{y}_{i-\text{LiDAR}}$  is an AGB prediction from a LiDAR-based model developed in L. K. Johnson et al. (2022).

### 2.4 Study area and parcel sample

NYS covers 141,297 km<sup>2</sup> in the northeastern US and was approximately 59% forested as of 2019 (USFS 2020). The forests are dominated by northern hardwoods-hemlock types but include Appalachian oak and beech-maple-basswood forests in the western and southern regions of the state respectively (Dyer 2006). The majority of NYS forests are privately owned (~73%; USDA Forest Service (2020)) and contained within parcels smaller than 40 ha (~65%; L'Roe and Allred (2013)). This already fragmented forest landscape is increasingly undergoing subdivision (L'Roe and Allred 2013).

To limit computational scope we selected a stratified random sample of ownership parcels within NYS. The statewide parcel database, compiled for property taxation, was obtained under agreement with the NYS ITS Geospatial Services. We stratified the statewide parcels into ten groups based on size, and five groups based on percent forest cover as determined by the United States Geological Survey's Land Change Monitoring, Assessment, and Projection (LCMAP) version 1.2 primary classification products (Zhu and Woodcock 2014; Brown et al. 2020). Size strata were selected to ensure a sample that represented a wide range of parcels, with an emphasis on smaller parcel sizes that dominate the NYS ownership landscape and are underrepresented in uncertainty estimation studies. Size strata were constructed as intervals (left-exclusive, right-inclusive) of parcel acreage as follows: (0, 5], (5, 10], (10, 20], (20, 50], (50, 100], (100, 250], (250, 500], (500, 1000], (1000, 2500], (2500, 5000]. Forest cover strata were selected such that a range of forest conditions were represented within each size stratum. Forest cover strata were constructed as five equal intervals from 0 (exclusive) to 100 (inclusive) percent. Forest cover was defined as the combination of the tree cover, wetlands, and grass/shrub LCMAP classes (L. K. Johnson et al. 2023). 50 parcels were randomly sampled from each size and cover group. For groups without 50 parcels, all available parcels were selected. Overall, 2224 parcels were sampled across the state (Figure 2).

### 2.5 Field data

The NYS FIA inventory data compiled in L. K. Johnson et al. (2023) were partitioned into model development (80%) and map assessment (20%) sets. The model development set was further partitioned into an 80% training set, and a 20% validation used for iterative assessment during model development. We used the model development partition to compute  $\text{Var}_{\text{boot}}$  (Section 2.2). This dataset included 1,954 completely forested plots, as well as 95 completely nonforested plots that were identified as true zeroes (AGB) based on LiDAR-derived maximum heights  $\leq 1$  m (L. K. Johnson et al. 2022), for a total of 2,049 plots inventoried between 2002 and 2019. We used the map assessment set to

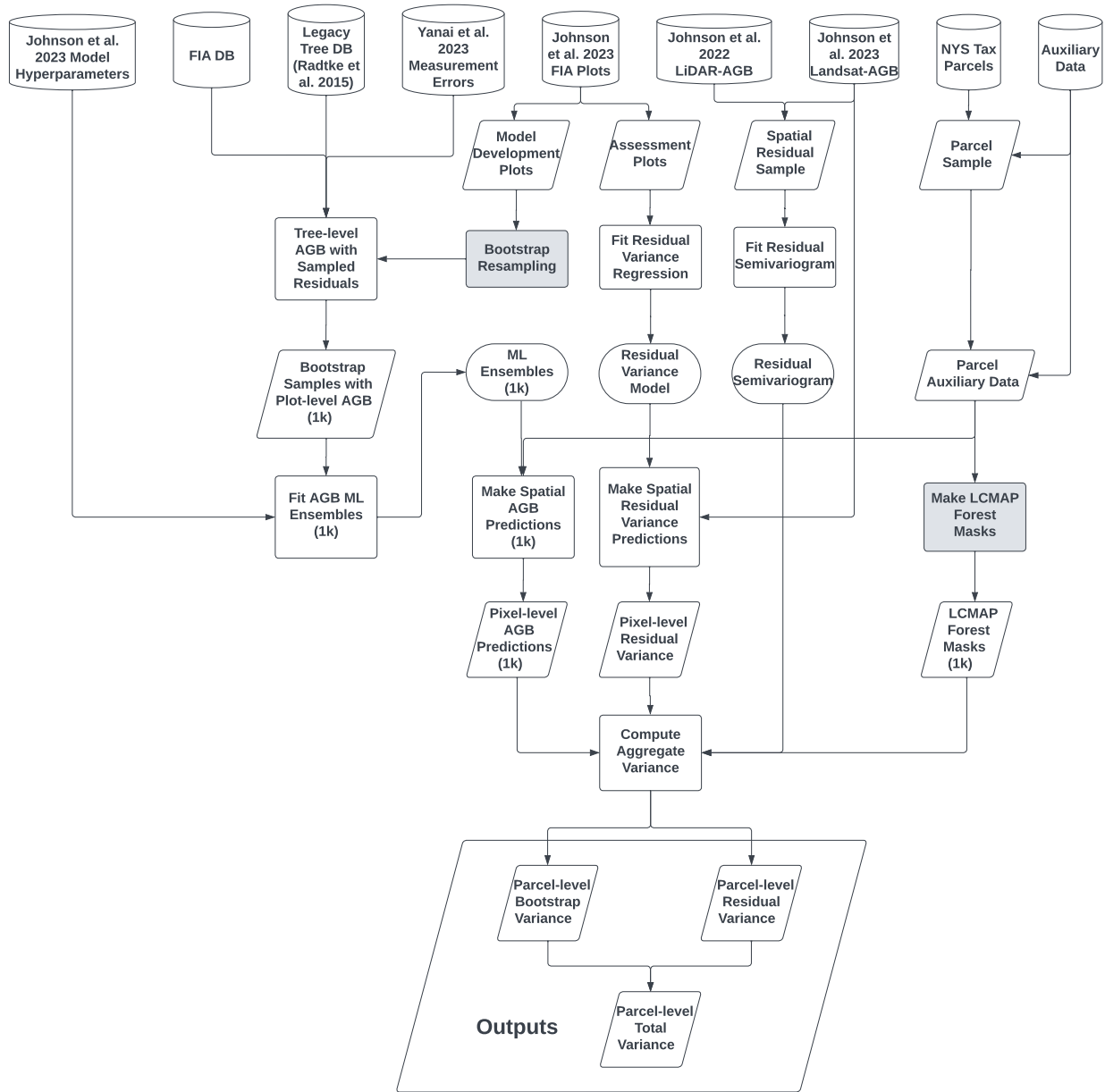


Figure 1: A flowchart showing the key elements of the methodology to estimate uncertainty for spatial means of aboveground biomass. Cylinders represent data sources, parallelograms represent data products and results, rectangles represent processing steps, and ovals represent models. Gray shaded nodes represent components that were omitted for separate runs of the workflow to further deconstruct  $Var_{boot}$  by subtraction into  $Var_{sam}$ ,  $Var_{LC}$ , and  $Var_{ref}$ .

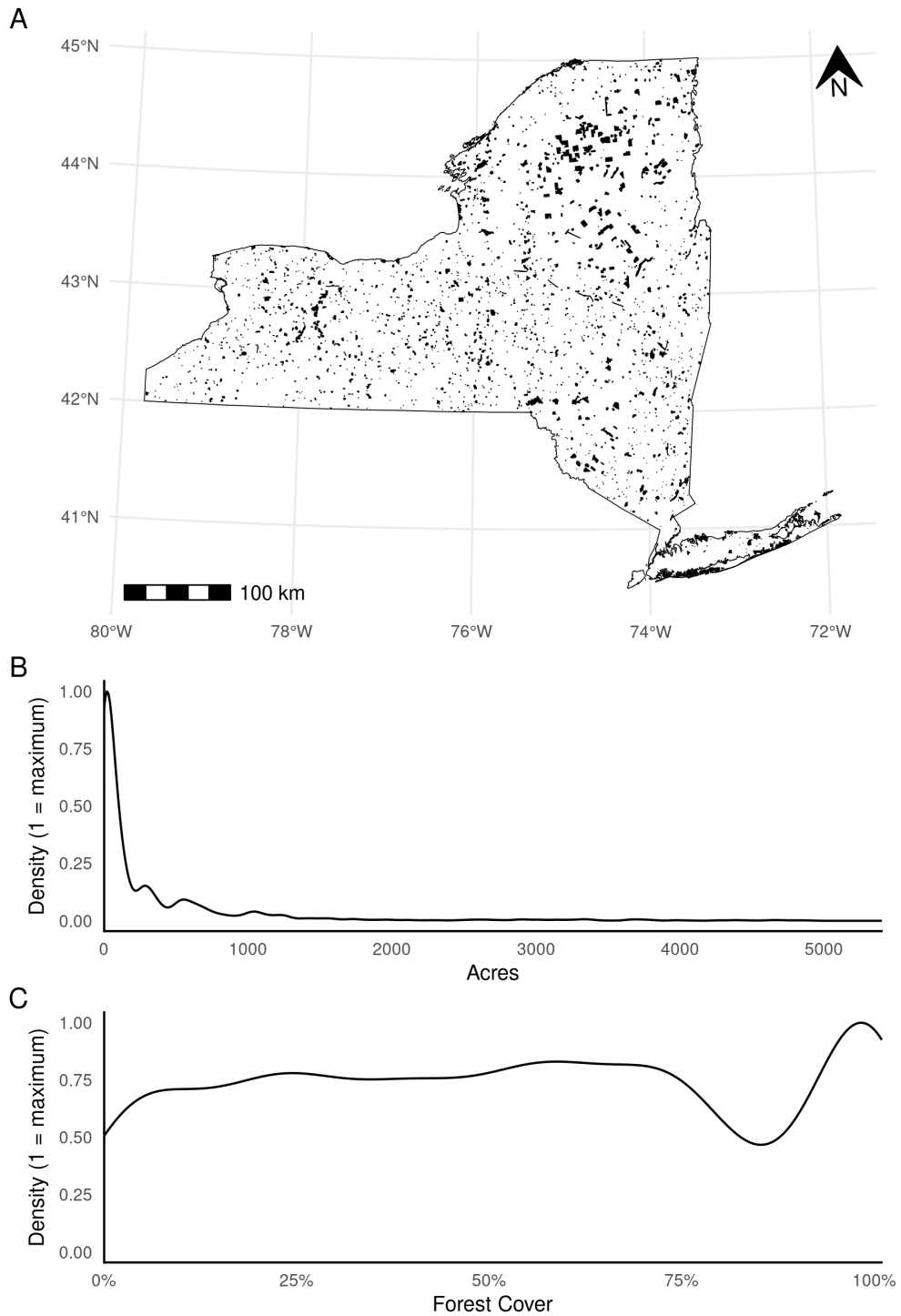


Figure 2: Parcel sample summary. A) Spatial distribution of sampled parcels within New York State. B) Smoothed frequency distribution of parcel sizes (acres) sampled. C) Smoothed frequency distribution of forest cover (%) sampled. Distributions for B and C have been rescaled separately, such that the most common occurrences of each variable are assigned a value of 1.



estimate the pixel-level residual variances (Section 2.8) that contribute to  $\text{Var}_{\text{res}}$  (Section 2.3). This dataset contained 545 plots inventoried in 2007, 2012, 2018, and 2019, collectively representing a complete spatial coverage of NYS. When plots in model development or map assessment sets were inventoried more than once, single instances were randomly selected so that each plot was associated with only one inventory year. Refer to L. K. Johnson et al. (2023) for further details on the FIA plot design and the plot selection criteria used here.

Rather than using the tree-level AGB predictions provided in the FIA database, we replicated FIA's component-ratio-method (CRM; Woodall et al. (2011)) to incorporate measurement error, misclassifications, and allometric uncertainty in the plot-level predictions. At the time of writing, FIA had transitioned to using a new system of allometric models (Westfall et al. 2023). However, our use of CRM remained consistent with the methods used in L. K. Johnson et al. (2023). A flowchart describing data inputs, component models, and final predictions for CRM is included in Appendix A.

For every bootstrap iteration we selected a set of plots with replacement from the model development partition, yielding as many sets of plots as bootstrap iterations. Further, for each plot and bootstrap iteration we constructed a plot polygon incorporating location uncertainty and computed plot-level biomass incorporating both measurement and classification errors as well as allometric uncertainty as detailed in the following sub-sections.

### 2.5.1 Measurement and classification error

Both measurement and classification errors were randomly selected and assigned to individual trees before summing tree-level predictions for each plot. We assumed normal distributions, despite representing (at best) approximations of true error distributions, for measured variables using parameters (mean, standard deviation) reported in the literature (Table 2). DECAECD misclassification was randomly assigned by selecting a random number between 0 and 1, and randomly choosing a sign (+/-). If the selected number was greater than the estimated 59% accuracy rate, then the decay class above or below was assigned based on the randomly selected sign (Table 3). Species classifications (SPCD in FIA DB), percent of bole volume that is represented by bark (BARK\_VOL\_PCT in FIA DB), and structural loss adjustments (Domke, Woodall, and Smith 2011) based on assigned decay codes (DECAECD in FIA DB) were omitted from tree-level uncertainty quantification due to lack of data or intractability. For example, misclassification rates for tree-level species were estimated by Yanai et al. (2023), but a method for assigning a replacement species in the event of a misclassification was not apparent.

### 2.5.2 Allometric model uncertainty

We utilized the legacy tree database, which provides records for volumes and weights of trees and tree components (e.g. foliage, top and branches, bole) for North American tree species (Radtke et al. 2015) to account for allometric model uncertainty. We selected only those records obtained from sites or studies within FIA's designated Northeastern states because the CRM models for NYS are specific to this region (Woodall et al. 2011). We used the database to produce separate hardwood and softwood empirical residual distributions for bole volume, bole bark biomass, bole wood biomass, foliage biomass, and total tree biomass (Appendix B). We did not account for stump biomass uncertainty or error since stump biomass measurements were not available for the Northeastern partition of the legacy tree database, and tractable estimates of uncertainty or error were not presented with the stump biomass models published in Raile (1982). All biomass residuals were computed relative to total tree biomass predicted with Jenkins et al. (2003) allometric models, and volume residuals were computed relative to predicted bole volume with Scott (1981) models so that adding randomly selected residuals would produce new estimates that were within a reasonable distance from the original.

Under the CRM approach, top and branch biomass (TAB) is predicted by subtracting all other predicted component biomass (stump, bole, foliage) from the predicted total. To ensure that our random residual selection yielded TAB estimates that were ecologically sound, we also compiled ratios of TAB to total tree biomass (minus predicted stump biomass; Appendix B) using the legacy tree database. We did not partition the TAB ratio distribution further into softwood and hardwood distributions since there were limited database records with both TAB measurements and total tree biomass measurements. Given the paucity of TAB ratio data, we filtered three records from the TAB ratio distribution where ratios were  $> 0.5$  to limit their influence on the overall outcome. After all components (total biomass, bole biomass, stump biomass, and foliage biomass) had been predicted and randomly selected residuals had been added to each component, we randomly selected a TAB ratio, computed a TAB prediction ( $[\text{TAB ratio}] \cdot [\text{total biomass}]$ ), and summed all components. The difference between the sum of components and the total was proportionally subtracted from each component to ensure that the sum of predicted component biomass was equal to the predicted total tree biomass.

### 2.5.3 Plot location uncertainty

FIA plots are composed of four identical circular subplots with radii of 7.32 m (24 ft), with one subplot centered at the macroplot centroid and three subplots located 36.6 m (120 ft) away at azimuths of 360°, 120°, and 240° (Bechtold and Patterson 2005). The FIA program averages individual plot locations collected over multiple repeat visits to improve

Table 2: Parameters and sources for estimating tree- and plot-level measurement error distributions. Where relative standard deviation (SD) is marked as ‘T’ (true), actual SDs are to be computed relative to the FIA provided value using the SD fraction in this table (i.e.  $\text{actualSD} = \text{SD}_{\text{table}} \cdot \text{FIA}_{\text{value}}$ ).

FIA DB Name	Description	Mean	SD	Rel. SD	Units	Source
DIA	Diameter at breast height	-0.004	0.55	F	cm	Yanai et al. 2023
BOLEHT	Bole height	-0.050	1.52	F	m	Yanai et al. 2023
CULL	Cull, percent rotten or missing	0.100	3.50	F	%	Yanai et al. 2023
WOOD_SPGR_GREENVOL_DRYWT	Wood specific gravity (green, oven-dry)	0.000	0.10	T	NA	Ross 2021
BARK_SPGR_GREENVOL_DRYWT	Bark specific gravity (green, oven-dry)	0.000	0.10	T	NA	Assumed
STANDING_DEAD_DECAY_RATIO (hardwood)	Hardwood density reduction ratios for DECAYCD 1-5	0.000	0.01 0.02 0.04 0.05 0.05	T	%	Harmon et al. 2011
STANDING_DEAD_DECAY_RATIO (softwood)	Softwood density reduction ratios for DECAYCD 1-5	0.000	0.01 0.01 0.03 0.03 0.03	T	%	Harmon et al. 2011
LON, LAT	Distance between field recorded plot location and plot location averaged over multiple repeat visits	0.000	7.05	F	m	NYS FIA DB

Table 3: Classification accuracies. User’s accuracy reported for LCMAP.

Name	Data Type	Description	Accuracy (%)	Source
DECAYCD	FIA	Tree-level decay code assigned in the field	59	Yanai et al. 2023
Developed	LCMAP	Primary landcover classification (LCPRI)	80	Stehman et al. 2021
Cropland			46	
Grass/shrub			37	
Tree cover			92	
Wetland			97	
Barren			1	

upon the precision and accuracy of field-recorded coordinates (Cooke 2000; Hoppus and Lister 2005). We constructed a normal distribution representing plot location errors by computing the standard deviation of differences between field-recorded coordinates and the corresponding average coordinates across all plots in the model development set (Table 2). To represent this positional uncertainty in  $\text{Var}_{\text{boot}}$  (specifically within  $\text{Var}_{\text{ref}}$ ), for each plot and at each bootstrap iteration, we randomly selected a distance  $d$  from the constructed normal distribution and a random azimuth  $a$  between  $0^\circ$  and  $360^\circ$  to create new plot centroids and subsequent plot polygons that were offset from the original plot centroid by a distance  $d$  m and an angle  $a^\circ$ .

## 2.6 Auxiliary data

We used the same set of 29 predictor layers derived in L. K. Johnson et al. (2023) for model training and mapping. These predictors included temporally segmented, gap-filled, and smoothed annual Landsat timeseries imagery and disturbance metrics (Landtrendr; Kennedy, Yang, and Cohen (2010), Kennedy, Yang, et al. (2018)), LCMAP primary and secondary landcover classifications, and static ecological, climatic, and topographic datasets. Each of the 29 predictor layers were projected to match Landsat 30 m pixel geometries. The raster stacks of predictors were cropped and aggregated (weighted average) at the constructed FIA plot polygons (Section 2.2; Section 2.5.3) to produce training

datasets, and were cropped to the boundaries of the parcels in our sample for mapping (Section 2.4). The exactextractr (Baston 2022) and terra (Hijmans 2023) packages for the R (R Core Team 2023) programming language were used to create the plot- and parcel-level auxiliary datasets. Further information describing the auxiliary data can be found in L. K. Johnson et al. (2023).

## 2.7 Aboveground biomass models, maps, and estimates

Following the ‘direct’ approach described in L. K. Johnson et al. (2023), ML ensemble models were fit to the resampled plots and corresponding AGB predictions for each bootstrap iteration (Section 2.2). Each ensemble was a linear regression that combined predictions from a random forest implemented with the ranger R package (Breiman 2001a; Wright and Ziegler 2017), a stochastic gradient boosting machine as implemented in the lightgbm R package (Friedman 2002; Ke et al. 2017; Shi et al. 2022), and a support vector machine (SVM) as implemented in the kernlab R package (Cortes and Vapnik 1995; Karatzoglou et al. 2004). We used the same set of hyperparameters, identified in L. K. Johnson et al. (2023) as the most performant via an iterative grid search, for each respective ML model across all bootstrap iterations. We used these pre-selected hyperparameters not only because the iterative grid search used in L. K. Johnson et al. (2023) was computationally expensive, but also because we do not expect the AGB or predictor distributions within each bootstrap sample to fundamentally differ since they represent the same underlying population. Further information describing the ML ensembles and hyperparameter tuning can be found in L. K. Johnson et al. (2023).

To compute  $\text{Var}_{\text{boot}}$ , an estimate of mean AGB for the parcel was computed for each iteration of the bootstrap (Section 2.2; Equation 3). To this end, separate sets of AGB predictions were made for all pixels within each sampled parcel using the models trained for each bootstrap iteration. Further, a separate forest mask was created and applied to each parcel for each bootstrap iteration to incorporate uncertainty and error in the LCMAP primary landcover classifications. New forest masks were produced at each iteration by generating a uniform random number between 0 and 1 for each pixel. If this number was greater than the user’s accuracy rate for the pixel’s initial classification (LCPRI), then the LCMAP secondary classification (LCSEC) was used instead (Table 3). After the new mask was generated, the mask was used to identify pixels that were not classified as tree cover, wetlands, or grass/shrub (forest definition from L. K. Johnson et al. (2023)) and set their AGB predictions to 0. After masking, and for each bootstrap iteration, parcel level means (Equation 4) were computed.

## 2.8 Residual variance model

Pixel-level residual variance was required to estimate  $\text{Var}_{\text{res}}$  (Section 2.3; Equation 9). However, residuals were only computed for a sample of pixels coinciding with FIA plots selected for the assessment partition from L. K. Johnson et al. (2023) (Section 2.5). Further, assigning the residual variance computed from this sample to every pixel would incorrectly assume homoscedasticity. To overcome this, we fit a model of estimated residual variance as a function of predicted AGB. Following the approach outlined in McRoberts et al. (2022), we arranged our assessment plots in order of increasing AGB prediction and partitioned the data into thirty equal AGB intervals ranging from 0 to the maximum AGB prediction in the dataset. To ensure a sufficient number of observations were available to estimate residual variance for each interval (McRoberts et al. 2022), we collapsed the initial groups until each interval contained at least 10 plots, resulting in 21 groups. We then computed the average AGB prediction and the residual variance for each group, and fit several forms of regression models relating AGB to residual variance for the 21 points in the dataset. Specifically, we evaluated linear, log-linear, log-log, third order polynomial, and natural cubic spline (2 knots, Hastie (1992)) model forms. The most basic (linear) model form was constructed as follows:

$$\hat{\sigma}_i^2 = \beta_0 + \beta_1 \cdot \hat{y}_i + \varepsilon \quad (12)$$

where  $\hat{y}_i$  is the average AGB prediction for the group,  $\hat{\sigma}_i^2$  is the estimated residual variance for the group, and  $\beta_0$  and  $\beta_1$  are coefficients estimated via ordinary least squares. All other model forms were fit similarly, using the same independent and dependent variables, but with log-transformations or additional model terms. When log transformations were used, we back-transformed estimates to a linear scale and applied multiplicative correction factors defined in Sprugel (1983) to eliminate log-transformation bias (Baskerville 1972) as follows:

$$\text{CF} = e^{\sigma^2/2} \quad (13)$$

where sigma is the residual standard deviation from the fitted model. We chose the model that best fit the data as indicated by the coefficient of determination ( $R^2$ ; computed after backtransformation and bias-correction), and then used this final model to estimate the residual variance for each pixel in our parcel sample.

## 2.9 Spatial autocorrelation of residuals

An estimate of spatial autocorrelation between model residuals was required to estimate  $\text{Var}_{\text{res}}$  (Section 2.3; Equation 9). However, the sample of assessment FIA plots used in L. K. Johnson et al. (2023), with at most one FIA plot per 2,400 ha in NYS (Bechtold and Patterson 2005), was too sparse to provide the necessary information. We instead used LiDAR-based predictions of AGB developed in L. K. Johnson et al. (2022) as an alternative form of reference data. We acknowledge that these predictions are of lesser quality than field-measured data, but they offered improved accuracy relative to the Landsat-based models assessed here, and they provided the spatial density and coverage that can represent local patterns of variability in forests. To our knowledge, these two important qualities are not offered by any other AGB dataset within NYS. We temporally and spatially matched Landsat-based maps with the spatiotemporal patchwork of LiDAR-based AGB predictions (L. K. Johnson et al. 2022) and selected a simple random sample of 500,000 pixels for which residuals were computed (Equation 11). We first calculated an empirical semivariogram from our sampled residuals with a bin width of 30 m (pixel resolution) which we then used to fit exponential, spherical, and Gaussian model semivariograms. We assessed the fits of each model semivariogram visually, and selected the best fitting model to use in Equation 10. All variogram computation and fitting was done with the `gstat` R package (Pebesma 2004; Gräler, Pebesma, and Heuvelink 2016).

To assess the sensitivity of our uncertainty estimates relative to the estimate of spatial autocorrelation between our LiDAR-based residuals, we computed four additional estimates of  $\text{Var}_{\text{res}}$  (Equation 9) where we multiplied pixel pairwise distances by 0.25, 0.5, 2, and by the estimated range of the semivariogram. In effect, these additional estimates of  $\text{Var}_{\text{res}}$  reflect residual spatial autocorrelation multiplied by a factor of 4, 2, 1/2, and 0 respectively.

## 2.10 Modeling estimated standard error (total variance) as a function of parcel characteristics

To increase the computational efficiency and practical utility of estimating spatially aggregated uncertainty for parcels or other subregions of interest, we modeled parcel SE as a function of parcel characteristics that we expect are readily available to map users. Specifically, we included AGB density, % forest cover, area, and perimeter of each parcel as predictors of a parcel's SE given that these predictors are straightforward to compute from an area of interest polygon, the AGB prediction raster, and a co-located forest mask raster. Forest cover was defined as the combination of the tree cover, wetlands, and grass/shrub LCMAP classes (L. K. Johnson et al. 2023), and AGB density ( $\text{Mg ha}^{-1}$ ) was computed as the average of pixel predictions within a parcel (Equation 4).

We fit four candidate models, one with no variable transformation, a second with natural log transformations for both the dependent and independent variables, and third and fourth models with natural log transformations for the dependent and independent variables respectively. When log transformations were used, we back-transformed estimates to a linear scale and applied correction factors (Equation 13) defined in Sprugel (1983) to eliminate log-transformation bias (Baskerville 1972). Candidate models were fit as follows:

$$\text{SE} = \beta_0 + \beta_1 \cdot \text{AGB} + \beta_2 \cdot \% \text{Forest} + \beta_3 \cdot \text{Area} + \beta_4 \cdot \text{Perimeter} + \varepsilon \quad (14)$$

where *AGB*, *% Forest*, *Area*, and *Perimeter* are described above and  $\beta_0, \dots, \beta_4$  are coefficients estimated via ordinary least squares. Each of the candidate models were fit to a randomly selected 80% of the parcel sample (training set) and were compared on the basis of  $R^2$ . The candidate model with the best  $R^2$  statistic was selected as the final model. Using the final model and the remaining 20% of the parcel sample (testing set) we computed model accuracy metrics including root mean squared error (RMSE), mean absolute error (MAE), mean error (ME), and  $R^2$  using the `yardstick` R package (Kuhn, Vaughan, and Hvitfeldt 2023). All model accuracy and comparison metrics were computed after any necessary backtransformation and bias-correction had been applied.

## 3 Results

### 3.1 Reference data uncertainty

Comparing the variability of tree- and plot-level AGB predictions provides insight into how allometric uncertainty and measurement error scales from individual trees to aggregations of many individuals within a plot. Over the 1000 bootstrap iterations tree-level AGB predictions varied more than plot-level AGB predictions (Appendix C). The average tree-level AGB standard deviation (SD) and coefficient of variation (CV) were 65.93 kg and 35.01%, while the average plot-level AGB SD and CV were 7.47  $\text{Mg ha}^{-1}$  and 7.20%. This result was unsurprising because plot-level predictions are simply area-normalized sums of tree-level predictions, and aggregating individuals can smooth out extreme individual variability as predictions above and below respective means will offset to an extent. Softwoods and hardwood trees varied similarly in absolute terms (SD), but softwoods varied substantially more in relative terms (CV).

### 3.2 Spatial autocorrelation of residuals

The exponential model semivariogram demonstrated the best fit to our empirical semivariogram (Section 2.9; Appendix D) and was selected to provide estimates of spatial correlation between model residuals in our calculation of  $\text{Var}_{\text{res}}$  (Equation 9). Residual semivariance increased from 199 ( $\text{Mg ha}^{-1}$ )<sup>2</sup> for neighboring pixels (nugget), to 1253 ( $\text{Mg ha}^{-1}$ )<sup>2</sup> (sill) for pixels roughly 1025 m (range) apart. Residual autocorrelation stops increasing beyond the estimated range and thus pixel pairs separated by distances greater than this range yielded  $\hat{\rho}_{ij} = 0$  (Equation 10).

### 3.3 Pixel-level uncertainty

The natural cubic spline model (Section 2.8) fit the grouped data best and explained 55% of the variability in residual variance (coefficient of determination;  $R^2$ ; Appendix E). Maps of pixel-level AGB estimates and co-located residual SEs (Figure 3 A) demonstrated the modeled relationship spatially, with regions of greater AGB density yielding larger residual SE estimates. Conversely, the largest sample and landcover SEs co-occurred within areas of consistently small AGB estimates (Figure 3 A). This sample SE pattern may be explained by the relative lack of model training data at the lower extreme of the distribution (L. K. Johnson et al. 2023) while the landcover SE pattern may be explained by the inclusion of LCMAP classification uncertainty in our bootstrapping procedure (Section 2.7). Marginal or transitional lands with relatively low AGB density are among the most challenging to accurately classify (Grass/Shrub and Cropland; Table 3) and may be intermittently masked to 0 AGB across bootstrap iterations. Pixel-level reference data SE was consistently near zero.

### 3.4 Spatially aggregated uncertainty estimates

Parcel-level estimates of standard error (SE; Equation 2) ranged from near 0  $\text{Mg ha}^{-1}$  to  $\sim 60 \text{ Mg ha}^{-1}$  but varied substantially with parcel size, forest cover, and AGB density (Figure 4; Figure 5). Although the range of SE was large, the majority of relative standard errors ( $\text{relSE} = \text{SE} / \text{AGB} \cdot 100$ ) were  $\leq 25\%$  and only exceeded 50% for  $\sim 7\%$  of parcels in the training partition (Figure 4). Parcels with the smallest AGB density yielded the largest relSEs.

Given that the formula for  $\text{Var}_{\text{res}}$  (Equation 9) contained  $N^2$  ( $N$  = number of pixels) in the denominator, it is intuitive that  $\text{Var}_{\text{total}}$  (Equation 1) and SE (Equation 2) decreased as a function of parcel size; the larger a parcel, the more 30 m pixels contained therein. Further, as parcel size grew beyond the range of spatial correlation and average pixel distances increased, it follows that  $\text{Var}_{\text{res}}$  decreased accordingly, and we might expect that  $\text{Var}_{\text{res}}$  will eventually become negligible for parcels larger than those considered in this study (Figure 6). Forest cover impacted parcel SE in the opposite direction (Figure 5), where increasing forest cover resulted in increased standard error. Non-forest pixels resulted in both 0 AGB and 0 residual variance; thus the greater number of these pixels in a parcel, the less forest cover and the smaller the contributions of  $\text{Var}_{\text{res}}$  to  $\text{Var}_{\text{total}}$ . However, the relationship between forest cover and SE may have been somewhat weakened by the impact of LCMAP classification uncertainty ( $\text{Var}_{\text{LC}}$ ), where the relatively poor accuracy of cropland and grass/shrub classified pixels may have yielded greater bootstrap variances as pixels were intermittently masked to 0 AGB across bootstrap iterations (Table 3; Section 2.7; Section 3.3).

$\text{Var}_{\text{res}}$  was greater than all other variance components across most size and forest cover groups (Figure 6). The contribution of  $\text{Var}_{\text{sam}}$  was only larger than  $\text{Var}_{\text{res}}$  for the largest parcels (2500 to 5000 acres) where spatial autocorrelation of residuals had a diminished impact.  $\text{Var}_{\text{LC}}$  contributed substantially ( $\geq 20\%$ ) for the least forested parcels, but contributed  $\leq 10\%$  for all but the smallest forest parcels.  $\text{Var}_{\text{ref}}$  contributed the least of any other component for all but the largest and most forested parcels (1000-5000 acres; 80-100% forested), and was always  $< 10\%$  of  $\text{Var}_{\text{total}}$ .

Parcel-level estimates of  $\text{Var}_{\text{total}}$  (and subsequently SE) were sensitive to the strength of residual spatial autocorrelation (Section 2.9; Figure 7). Adjustment factors that strengthened residual autocorrelation had the smallest impact for small parcels, where the majority of pair-wise pixel distances were short and residual spatial autocorrelation already had a near-maximum impact. On the other hand, strengthening residual autocorrelation increased  $\text{Var}_{\text{total}}$  by  $\geq 50\%$  for all size groups  $\geq 20$  acres. Halving the strength of residual spatial correlation reduced  $\text{Var}_{\text{total}}$  from 15.7% to 48.0%, and removing residual spatial correlation altogether reduced  $\text{Var}_{\text{total}}$  from 38.1% to 80.7%. This highlights the importance of residual spatial autocorrelation as a source of uncertainty when estimating SE for small areas.

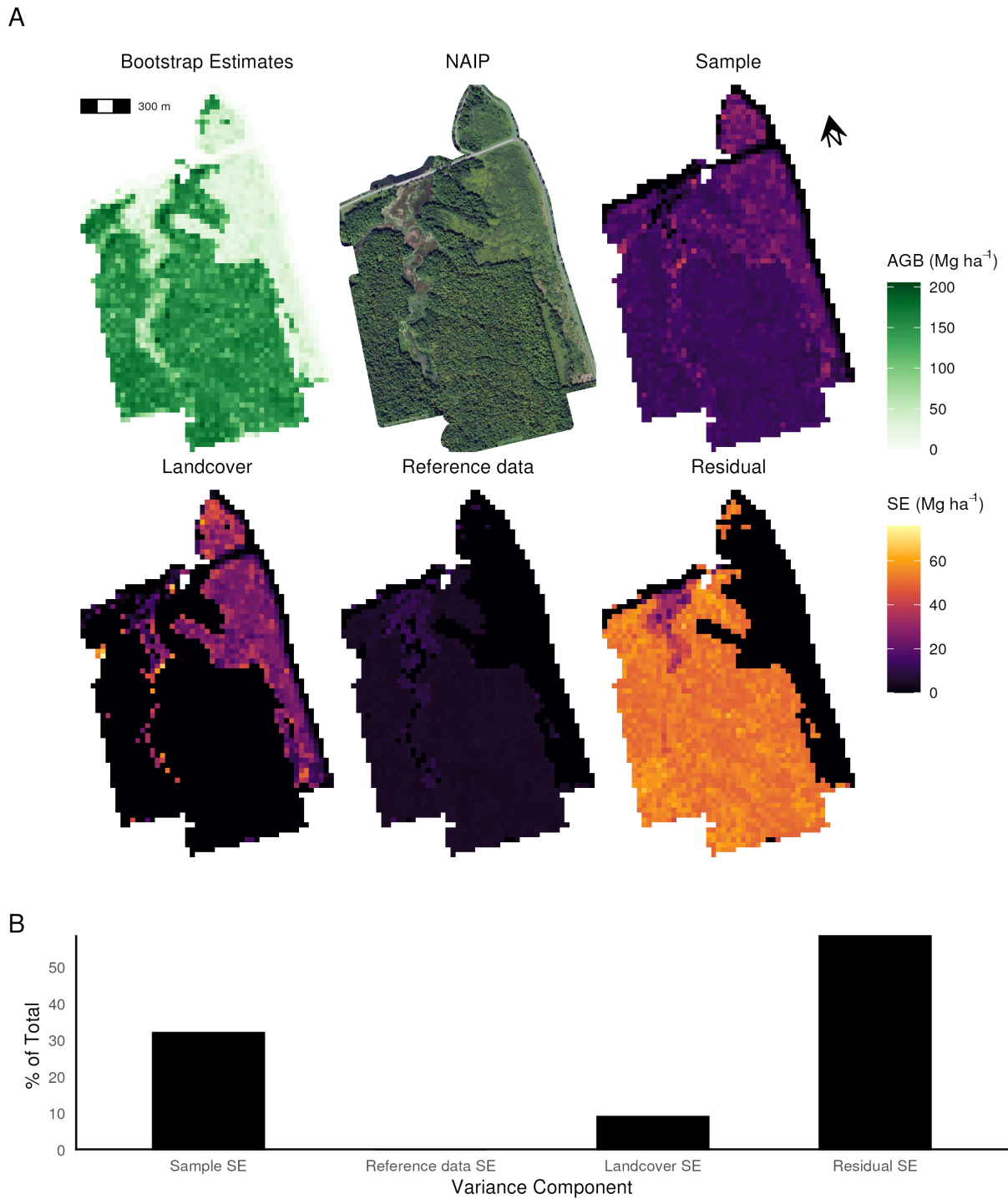


Figure 3: Aggregating pixel-level uncertainties to produce parcel-level standard error (SE). A) Bootstrap estimates: AGB estimates computed as the mean prediction over all bootstrap iterations. National Aerial Imagery Program (NAIP) orthophotography collected in 2019 for additional reference. Sampling standard error (SE), landcover SE, reference SE, and residual SE estimates. B) Relative contributions (%) to total SE for the area of interest in A.

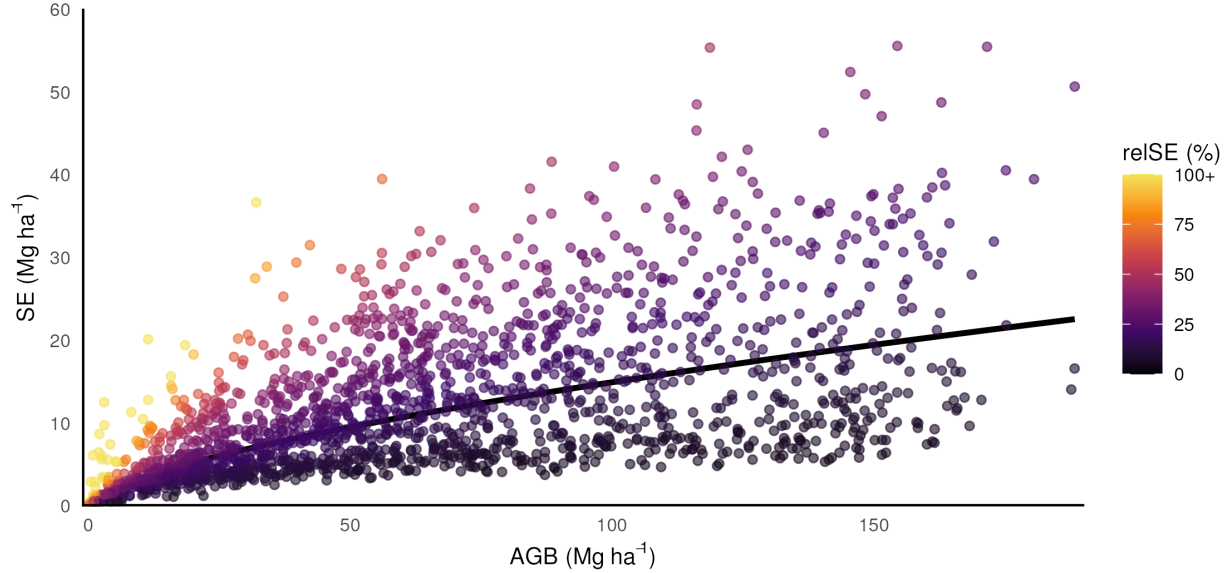


Figure 4: Parcel-level standard error (SE) as a function of AGB density. Each point represents a parcel from the training partition of the parcel sample, and each point is shaded by the relative standard error (reISE;  $(SE / AGB) \cdot 100$ ). Parcels with reISE > 100% were set to 100% for visualization. The black trend line was fit to data using a natural log-log regression.

Table 4: Results of a natural log-log regression model of estimated parcel-level standard error as a function of parcel characteristics (AGB, Perimeter, Area, and % Forest).

	Coefficient	Standard error	t	p
Intercept	1.298	0.088	14.8	< 0.001
ln(AGB)	0.584	0.006	105.4	< 0.001
ln(Perimeter)	-0.167	0.014	-12.0	< 0.001
ln(Area)	-0.146	0.008	-17.9	< 0.001
ln(% Forest)	0.123	0.005	26.7	< 0.001

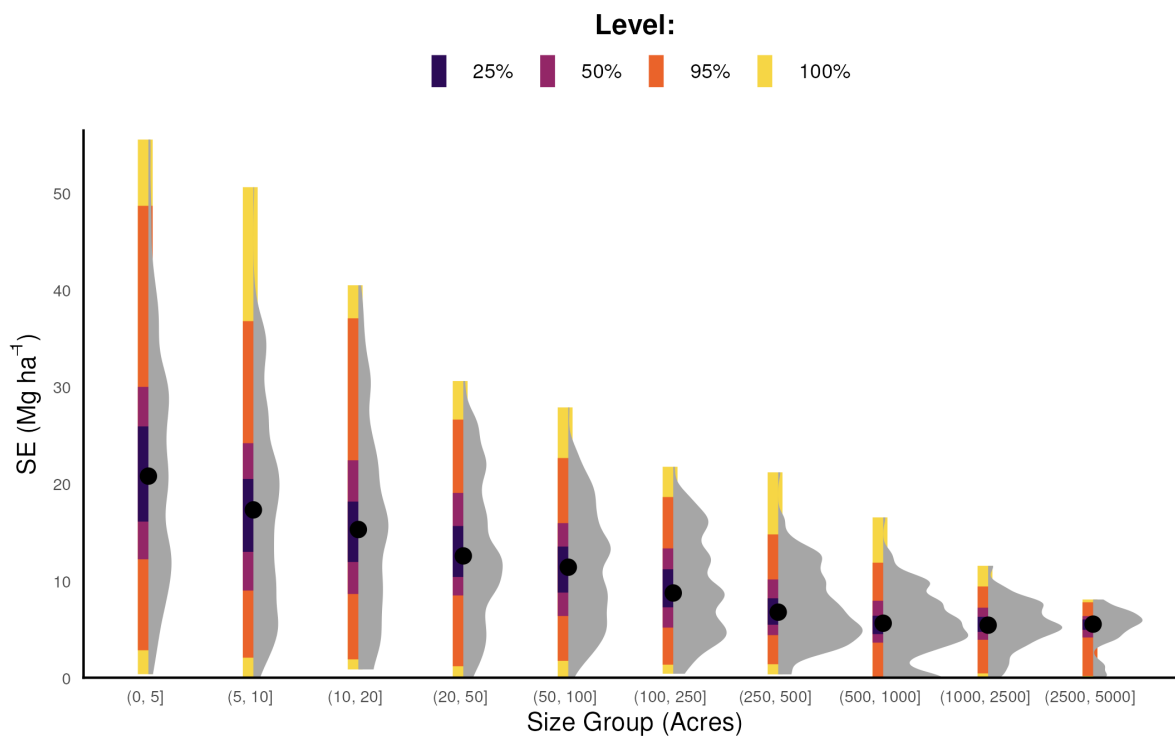
### 3.5 Modeling estimated standard error (total variance) as a function of parcel characteristics

The natural log-log regression achieved the best  $R^2$  value among the candidate models (Section 2.10) and accurately estimated SEs for parcels in the test set (Appendix F; RMSE = 2.46, MAE = 1.38, ME = -0.21,  $R^2 = 0.93$ ). The estimated coefficients (Table 4) indicate that AGB density was the most important predictor of SE, which follows the relationship inherent to our residual variance model (Section 2.8; Appendix E) and is corroborated by both pixel-level results (Figure 3) and reISE results (Figure 4). Parcel area, perimeter, and % forest cover were similarly important predictors in the model. Using this model we estimated parcel-level SE for all ownership parcels in Essex County, New York State (NYS; Figure 8).

## 4 Discussion

In this study we produced model-based estimates of uncertainty (standard error; SE) for small-area (<1-5000 acres) spatial averages of forest aboveground biomass (AGB) maps. Our SE estimation approach uniquely included all four types of uncertainty (Table 1), was compatible with algorithmic models (machine learning or nonparametric), and incorporated residual spatial autocorrelation. We found that residual variance ( $Var_{res}$ ; Equation 9) dominated other variance components for all but the largest parcels (2500-5000 acres), owing largely to contributions from residual spatial autocorrelation (Figure 7). These results underscore the necessity of incorporating residual spatial autocorrelation when estimating uncertainty at scales germane to forest management (e.g. parcel sizes in New York state). We demonstrated that a log-log regression model for estimating SE as a function of parcel characteristics was very accurate, opening the door to more computationally efficient and practical uncertainty estimation for map subregions. Overall, these findings

A



B

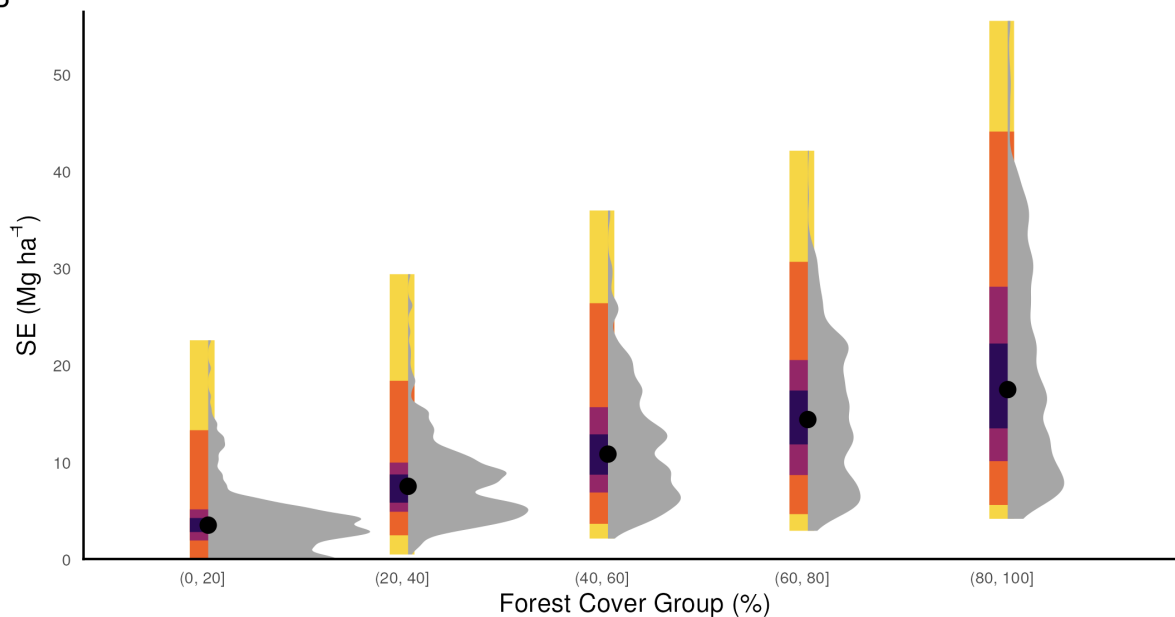
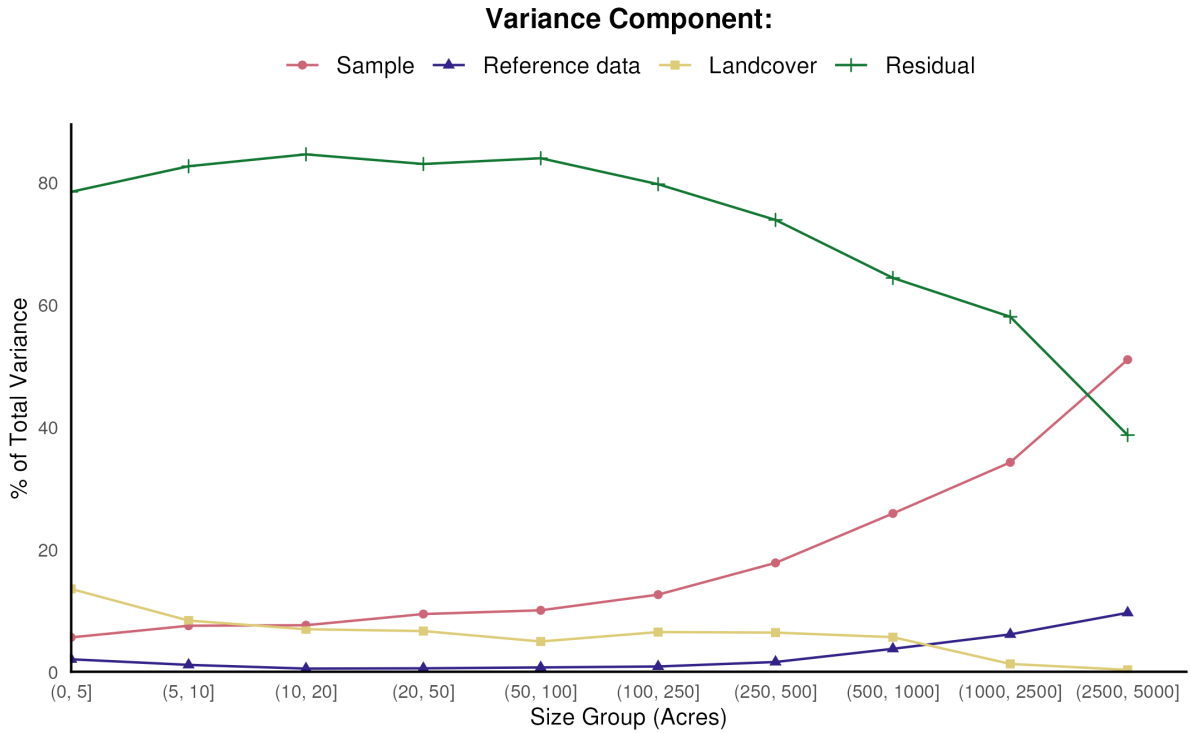


Figure 5: Parcel-level standard error (SE) distributions. Gray shaded areas represent smoothed frequency distributions of SEs, black dots identify median values, and colored bars show 25%, 50%, 95%, and 100% intervals (percentiles). A) Distributions per size group (acre). B) Distributions per forest cover group (%). All parcels in the training partition of the parcel sample are included.



A



B

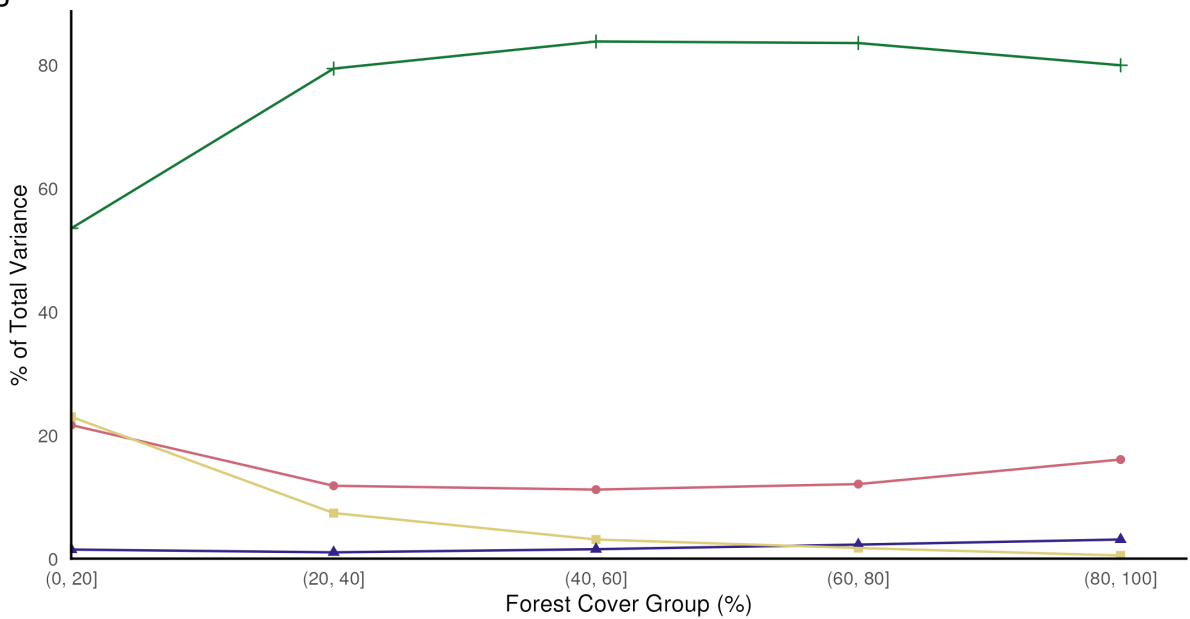


Figure 6: Uncertainty contributions (% of total variance) as a function of parcel size (A) and forest cover (B) for the training partition of the parcel sample. For each source of uncertainty, the average percent of the total variance was summarized across all parcels within each group.

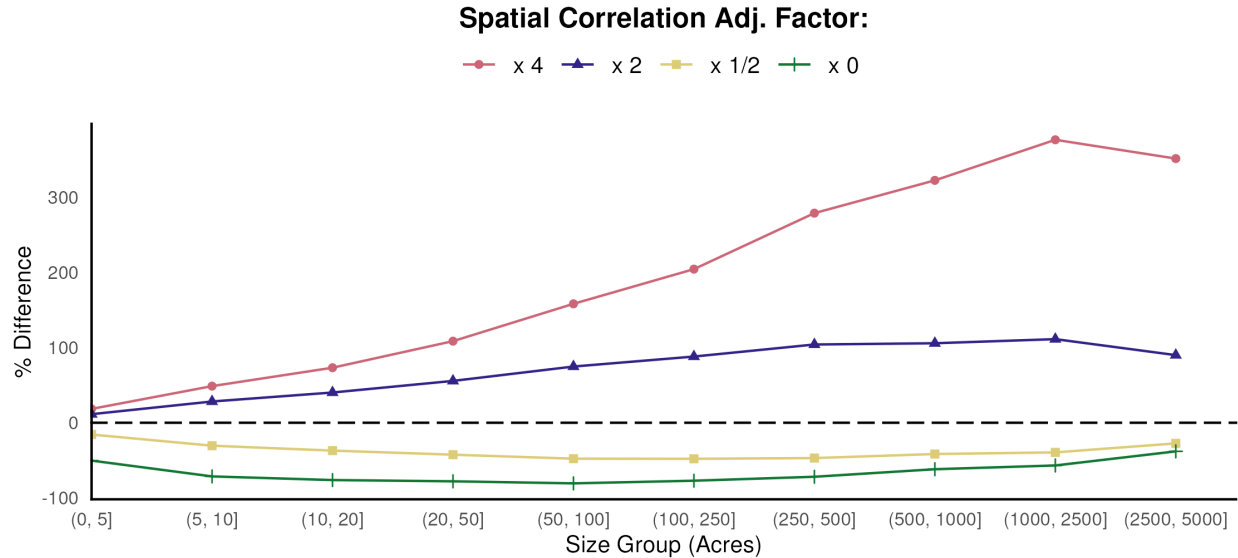


Figure 7: Sensitivity of total variance estimates to strength of residual spatial autocorrelation. Percent difference between total variance adjusted for strengthened/weakened spatial correlation of residuals (adjustment factor  $\neq 1$ ) and total variance computed regularly (adjustment factor = 1; dashed black line) as a function of parcel size (size group) for the training partition of the parcel sample. The average percent difference was summarized across all parcels within each group. Spatial correlation adjustment factors are used to modify the pairwise pixel distances (e.g. adjustment factor 4 is implemented by dividing the pairwise pixel residual distances by 4) such that the adjustment factor effectively describes a multiplicative adjustment to the empirical spatial correlation of residuals.

pave the way for rigorous uncertainty estimation in future regional-scale model-based forest carbon accounting and monitoring efforts.

#### 4.1 Contributions to total uncertainty

Attributing contributions to total uncertainty from various sources is a critical step to reducing uncertainty, one of the IPCC good practice guidelines (“uncertainties are reduced as far as practicable”; Buendia et al. (2019)). Without identifying sources of uncertainty, reduction efforts cannot be effectively directed. Although these results most directly inform reducing uncertainties associated with the specific modeling framework implemented in L. K. Johnson et al. (2023), the general patterns uncovered here may also serve to inform future model-based efforts insofar as sufficient overlap exists in terms of sampling designs, reference data collection protocols, remotely sensed data products, and model forms.

Residual variance ( $\text{Var}_{\text{res}}$ ; Equation 9) dominated all sources of uncertainty for all but the largest parcel sizes (0-2500 acres; Figure 6) primarily due to the impact of model residual spatial autocorrelation (Figure 7). These results hold significance for future model-based efforts in areas where forests are divided into smaller units and parcel dimensions do not far exceed the range of spatial autocorrelation. In regions like the eastern and midwestern United States (US), forests are predominantly managed by nonindustrial private forest owners (“family forests”), and these family forest holdings are often small (Nelson, Liknes, and Butler 2010; Butler et al. 2016). We therefore recommend prioritizing model accuracy to most effectively reduce total uncertainty ( $\text{Var}_{\text{total}}$ , Equation 1; SE, Equation 2) in these contexts. Increased model accuracy simultaneously reduces both residual variance and residual spatial autocorrelation, effectively diminishing  $\text{Var}_{\text{res}}$ . Of course, model accuracy is almost always a priority, but we highlight its importance relative to other uncertainty components assuming a limited amount of time and resources with which to reduce total variance (Table 1). In particular, the inclusion of data from active remote sensing systems, like synthetic aperture radar or spaceborne LiDAR which can penetrate forest canopies and may better represent structural attributes related to AGB, could increase model accuracy (Quegan et al. 2019; Dubayah et al. 2020). Higher resolution imagery in concert with the implementation of deep-learning algorithms like convolutional neural networks which can exploit local spatial patterns may offer improved model predictions as well (LeCun, Bengio, and Hinton 2015; Kattenborn et al. 2021).

Sampling variance ( $\text{Var}_{\text{sam}}$ ; Equation 6) was the largest contributor to total uncertainty for only the largest parcels (2500-5000 acres; Figure 6). We expect this to hold true for NYS parcels larger than the maximum size considered in

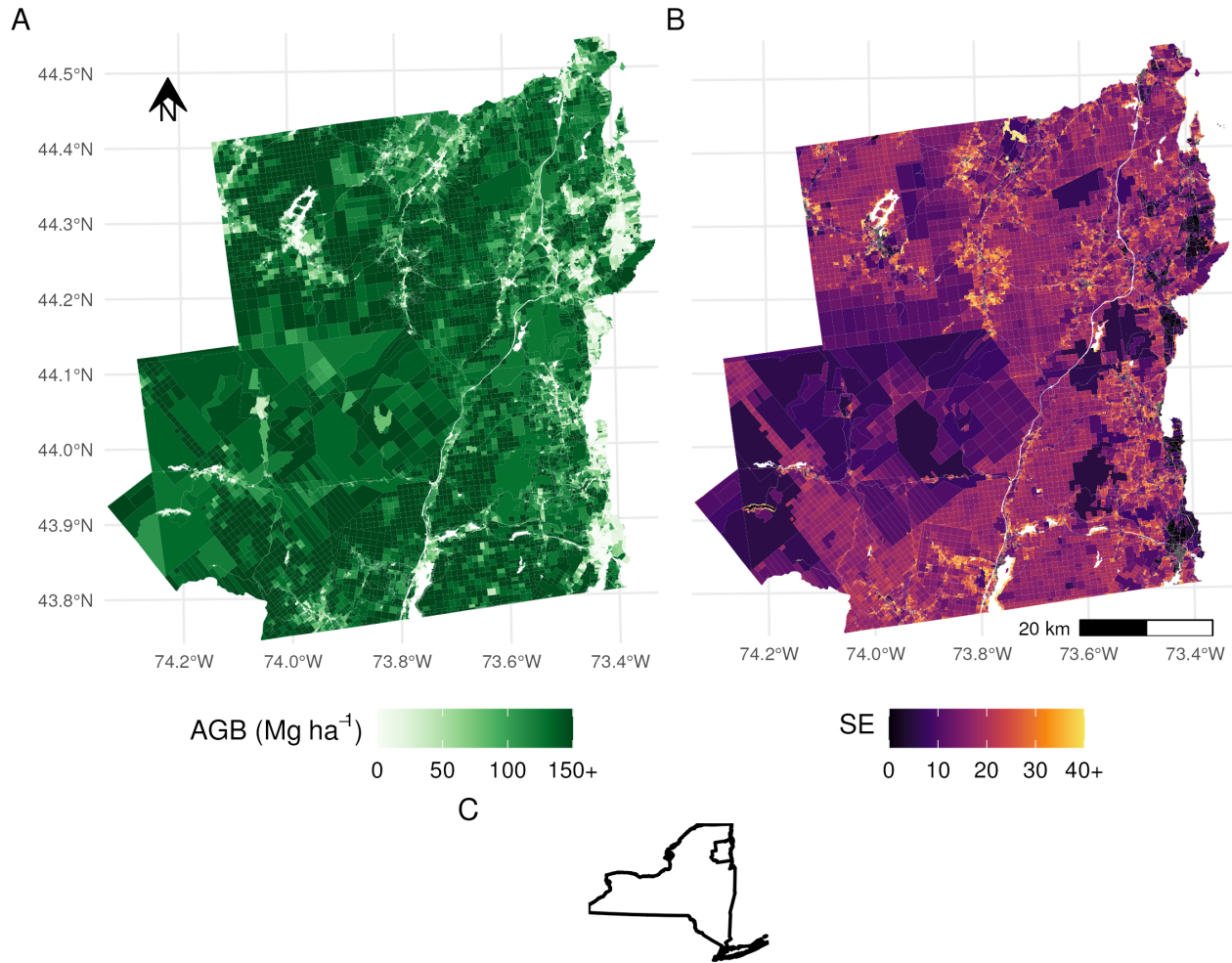


Figure 8: Estimates of aboveground biomass density and associated standard error for ownership parcels in Essex County, NYS. A) Parcel-level AGB density computed as the mean of pixel-predictions within each parcel. B) Parcel-level SE estimated from a natural log-log regression with parcel area, perimeter, AGB density, and % forest cover as independent variables. C) Location of Essex County within NYS. AGB density and SE values truncated at 150 and 40 respectively for display.

this study given the inverse relationship between  $\text{Var}_{\text{res}}$  and parcel size. In other words, while we assume  $\text{Var}_{\text{res}}$  will approach zero with increasing parcel size, we also assume that  $\text{Var}_{\text{sam}}$  will remain relatively stable and thus contribute a larger and larger proportion to a decreasing  $\text{Var}_{\text{total}}$ . With all other variables held constant, this suggests that in regions where forests are contained in larger contiguous management units, like the western US (Nelson, Liknes, and Butler 2010; Butler et al. 2016), reductions in model-based uncertainty can be most efficiently achieved by investing in more forest inventory sample locations. However, forests in the western US are generally conifer-dominated with even-aged disturbance regimes (Perry et al. 2022; Rogers 1996), whereas forests in the eastern US are mostly mixed hardwood-conifer with uneven-aged disturbance regimes (Seymour, White, and deMaynadier 2002; Dyer 2006). As a result, it is entirely possible that spatial correlation of model residuals may be stronger across the larger and more uniform patches of forest in the West, suggesting that reducing residual variance ( $\text{Var}_{\text{res}}$ ) instead of sampling variance ( $\text{Var}_{\text{sam}}$ ) may be the most efficient means to reduce total variance. That said, eastern and western forests of the US may be too distinct to be able to extrapolate drivers of model-based variability from one region to the other.

Contributions from landcover mask variability ( $\text{Var}_{\text{LC}}$ ; Equation 7) were small except in the least forested parcels (0-20% forested; > 20% of  $\text{Var}_{\text{total}}$ ; Figure 6). We can infer that the increased landcover variability in these parcels is tied to the presence of marginal and transitional landcover classes (e.g. grass/shrub, cropland), which in many contexts may hold non-trivial quantities of forest biomass (Schnell et al. 2014; K. D. Johnson et al. 2015; S. Liu et al. 2023), but are traditionally challenging to classify (Table 3; Brown et al. (2020), Stehman et al. (2021), Mahoney et al.

(2022)). Subsequently, we suggest that landcover classification accuracy and precision may be worth prioritizing in areas dominated by woodlands, shrublands, other marginal, transitional, or novel land cover types, or where agroforestry is commonplace (Van Auken 2000; Knapp et al. 2007; Schoeneberger 2009; Udawatta and Jose 2011; Mahoney et al. 2022).

Reference data variability ( $\text{Var}_{\text{ref}}$ ; Equation 8) contributed minimally to total uncertainty across all analyzed groupings (Figure 6;  $< 10\%$  of  $\text{Var}_{\text{total}}$ ). These results corroborate previous studies reporting that tree-level uncertainty contributes minimally to total uncertainty when aggregated over many individuals (Breidenbach et al. 2014; Ståhl et al. 2014; McRoberts and Westfall 2014; Yanai et al. 2023); indeed, we demonstrated that the coefficient of variation (CV) for plot-level AGB was an order of magnitude smaller than the CV for tree-level AGB (tree-level AGB CV 35.01%; plot-level AGB CV 7.2%) despite relying on relatively small-area plots (0.067 ha). One would expect even less variability if larger area plots were utilized (as recommended by CEOS (2021)). Further, our results suggest that the imprecision of FIA plot locations (7.05 m standard deviation; Table 2) does not meaningfully impact total uncertainty. We might infer that the fidelity of 30 m Landsat imagery is not adequate, or that forests in NYS are not sufficiently patchy for imprecise reference data geolocation to be meaningful in this context. Despite its relative lack of importance in this study, reference data uncertainty may be important in regions where only small fractions of the tree population are represented in the data used to fit the allometric model. Regions like the global tropics with a greater diversity of tree species (Chave et al. 2014) or regions with a scarcity of forest inventory plots due to remoteness or lack of resources (e.g., lacking a national forest inventory; McRoberts, Tomppo, and Næsset (2010)) could yield particularly large reference data uncertainty contributions. It is therefore prudent to weigh the precision and representativeness (Labrière et al. 2022) of a given system of allometric models against the practicality and feasibility of incorporating reference data uncertainty in estimates of total variance.

In general, the framework we have developed may facilitate a range of sensitivity analyses for different components of uncertainty and parameters not limited to those considered here. By keeping all other inputs constant, and increasing (or conversely removing) uncertainty from a single component, we can begin to identify specific thresholds beyond which more granular uncertainty contributions overwhelm the total uncertainty estimate. Although these kinds of analyses may be simple in theory, they are computationally expensive, as testing each component requires a new 1000 iteration bootstrap procedure. With further investments and developments in computational infrastructure such analyses may become more tractable. Nevertheless, we recommend this kind of framework for iteratively exploring sources of model-based uncertainty.

## 4.2 Communicating uncertainty to map users

Although pixel-level predictions in fine-resolution maps effectively represent spatial patterns, finer resolution is often associated with increased uncertainty, and management decisions are made at coarser spatial scales. Thus we expect that users will spatially aggregate groups of pixels into units representing forest stands, ownership parcels, or other practically relevant units for formal estimation. The delivery of corresponding uncertainty maps (pixel-level variance) alone fails to facilitate statistically sound estimates of aggregate uncertainty, as pixel-level variances cannot be naively averaged within areas of interest in the same way that AGB predictions can (Wadoux and Heuvelink 2023). We therefore explored alternative ways to communicate the methods and metadata required to make rigorous uncertainty estimates for map subregions.

In this study we found that parcel-level uncertainty (SE) varied substantially with parcel size, forest cover, and AGB density, thus enabling the use of a natural log-log multiple regression (Table 4; Appendix F) for accurately estimating SE for any subregion of the AGB maps from L. K. Johnson et al. (2023). Given the coefficients of this regression, map users need only compute the predictors for their area of interest and substitute them into the model formula (Equation 14). All of the parcel characteristics included as predictors in the model are intended to be accessible to map users since each can be computed with a standard GIS and a bounding polygon for the user's area of interest.

We do not expect that this type of regression will be useful across all landscapes, ecological domains, or modeling frameworks. However, we do expect this type of regression to be most effective for models that exhibit heteroscedastic residual variance, or in regions where the majority of estimation unit sizes are relatively small. In these situations, both the positive correlation between AGB and residual variance and the strong inverse relationship between estimation unit size and spatial covariance of residuals ( $\text{Var}_{\text{res}}$ ; Equation 9) can be leveraged to make accurate estimates. In regions with constant residual variance, or where the majority of estimation units have dimensions that exceed the range of spatial autocorrelation of residuals, this type of regression may be less effective at estimating SE. However, we expect SEs in these circumstances to be generally small. Further, bootstrap variance ( $\text{Var}_{\text{boot}}$ ; Equation 3) may contribute more substantially in regions with more sparsely sampled forest inventories ( $\text{Var}_{\text{sam}}$ ) or less precise allometric models ( $\text{Var}_{\text{ref}}$ ). In these contexts, alternative predictors that help describe the degree to which a subregion is represented in the reference data or forest inventory sample may be useful (e.g. area of applicability information; Meyer and Pebesma

(2021)). In light of our findings, we recommend further investigation into regression as a means to communicate uncertainty for map subregions in a diversity of contexts.

Improving the transfer of uncertainty information to map users enables a more rigorous application of map products in decision-support contexts. Specifically, the estimates of SE produced in this study provide managers and decision-makers the means to compare the outcomes of various policies and management practices across the landscape with the added context of confidence intervals (Figure 8). For example, the hypothesis that forests protected by conservation easements hold larger carbon stocks can be formally tested (McRoberts 2011). Although this study has focused entirely on estimating uncertainties associated with AGB stocks, the same bootstrapping approach and the parcel-level SE estimates developed here may facilitate the estimation of uncertainties associated with stock-changes (Esteban et al. 2020), which can explicitly account for GHG emissions and removals attributed to the forest sector and can be used to track forest carbon dynamics through time.

### 4.3 Limitations

Although this study demonstrates rigorous uncertainty estimation, our approach is not without limitations and assumptions. In general, there is a degree of subjectivity involved in choosing which sources of uncertainty are included in an assessment. Here we have omitted uncertainty in model predictor data (Table 1, type d) from our framework (CEOS 2021). The models in L. K. Johnson et al. (2023) are largely dependent on Landsat imagery that has been temporally smoothed, segmented, and gap-filled by Landtreindr (Kennedy, Yang, and Cohen 2010; Kennedy, Yang, et al. 2018). Although incorporating uncertainty associated with the geometric or radiometric features of the raw Landsat imagery was beyond the scope of this study, we may be able to use the Landtreindr residuals (differences between raw spectral value and Landtreindr fitted value) to assess variability in the imagery in future studies. In consideration of computational efficiency, we limited the number of bootstrap iterations to 1000. McRoberts et al. (2023) proved a formal bootstrap stopping criterion that could be applied to ensure precise and accurate estimates of SE but also demonstrated that 1000 is often within the range of bootstrap iterations that can produce reliable SE estimates. In light of data availability and project efficiency, we relied on published statistics to build normal distributions of measurement errors rather than sampling from empirical distributions (Table 2). While these assumed normal distributions are, at best, approximations of true error distributions, we deemed them acceptable given that reference data uncertainty is often ignored due to overall intractability. We used LiDAR-based predictions of AGB as reference data when estimating residual spatial autocorrelation instead of field inventory reference data (Section 2.9). Although estimates of parcel-level SE are sensitive to the strength of residual spatial correlation (Figure 7) and there is no guarantee that residuals computed with LiDAR-based reference data have the same spatial properties as those computed with field inventory data, this substitution was a practical solution to achieve the spatial density and coverage required for estimating residual spatial autocorrelation. Finally, other bootstrapping protocols may be more desirable within the circumstances of our study. In our case we have blended pairs bootstrapping (resampling plots with replacement) and residual bootstrapping (FIA plots; measurement errors, allometric errors, and plot location errors) within the same iterative framework (Efron and Tibshirani 1994). Wild bootstrapping (Esteban et al. 2020; R. Y. Liu 1988) may be preferred as it preserves both the original sampling structure and the heteroskedasticity of model residuals.

## 5 Conclusion

The proliferation of fine-resolution forest biomass (AGB) and carbon maps has not been matched with corresponding effort in the estimation and communication of uncertainty for small-area spatial aggregates of map subregions. To address this shortcoming, we developed and applied methodology to produce estimates of standard error (SE) associated with spatial averages of AGB predictions for a stratified random sample of ownership parcels in New York State. This represents a novel model-based uncertainty estimation approach that included all four types of uncertainty (Table 1), that used methods compatible with algorithmic models (machine learning or nonparametric), and that incorporated spatial autocorrelation of residuals. Our results suggest that residual variance, largely resulting from spatial autocorrelation of model residuals, will be the largest source of uncertainty in landscapes like the midwestern and northeastern United States where forests are divided into smaller ownership units. This highlights the importance of accounting for residual spatial autocorrelation in small-area uncertainty estimates, and implies that improvements in model accuracy will yield the greatest reductions to uncertainty in these regions. We further demonstrated that a regression model relating parcel characteristics (area, perimeter, AGB density, forest cover) to parcel SE can provide accurate uncertainty estimation for any map subregion with only a fraction of the computing resources and data required to do so from first principles. Overall, our approach and outputs can directly support future regional-scale model-based efforts and promote transparency in spatial forest carbon accounting.

## **6 Acknowledgements**

We would like to thank the USDA Forest Service FIA program for their data sharing and cooperation, and especially Brian F. Walters for his consultation. We would also like to thank Sean Healey for his helpful comments, the NYS GPO for compiling and serving LiDAR data, and the NYS Department of Environmental Conservation (#AM11459), Office of Climate Change for funding support. The findings and conclusions in this publication are those of the author(s) and should not be construed to represent any official US Department of Agriculture or US Government determination or policy.

Appendix A: Component ratio method

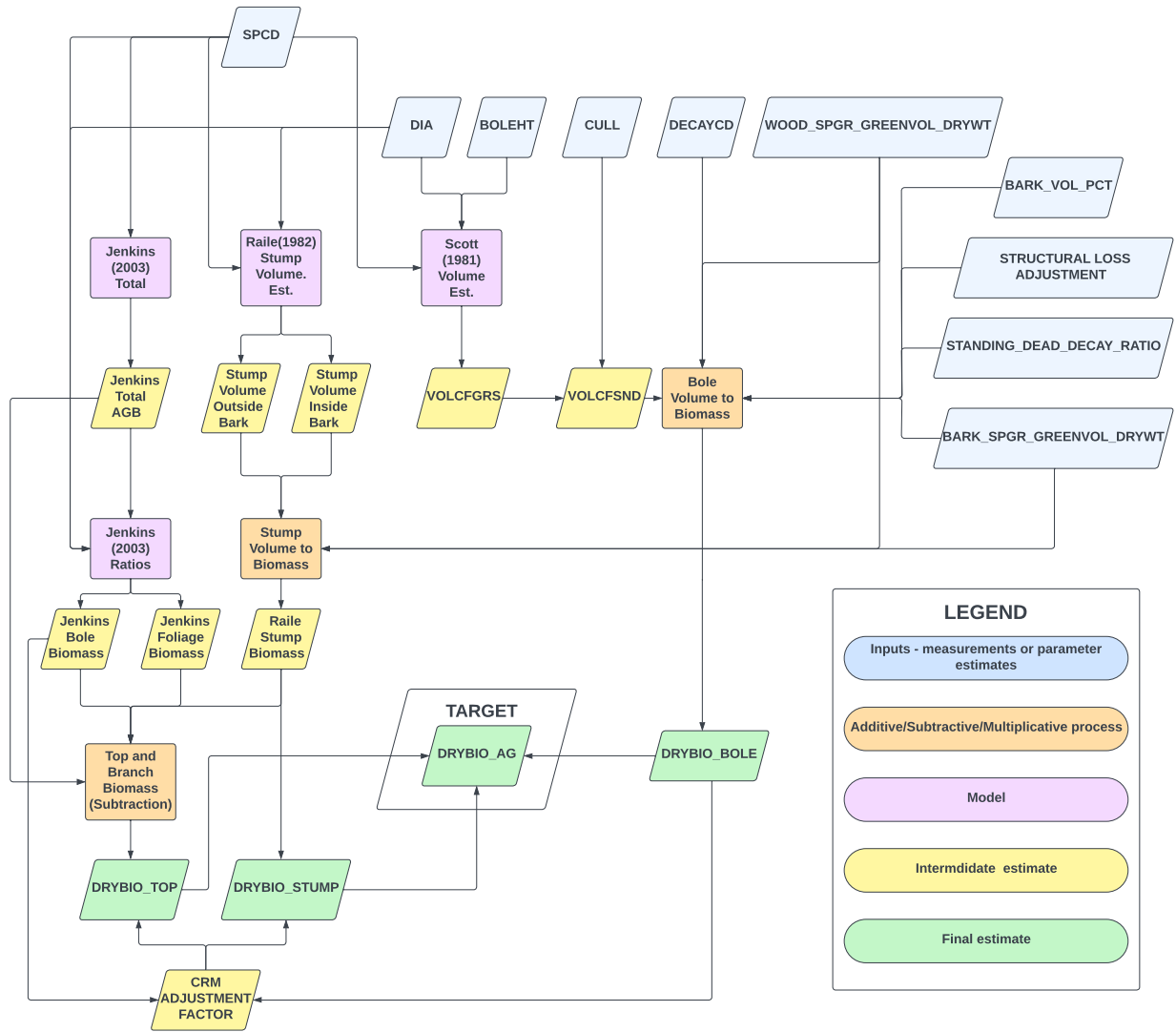


Figure A1: Flowchart showing key elements of the component ratio method (CRM; Woodall et al. 2011) for estimating tree-level AGB (DRYBIO\_AG) using the FIA database. All names of inputs reflect FIA database values as best as possible.

## Appendix B: Legacy tree database

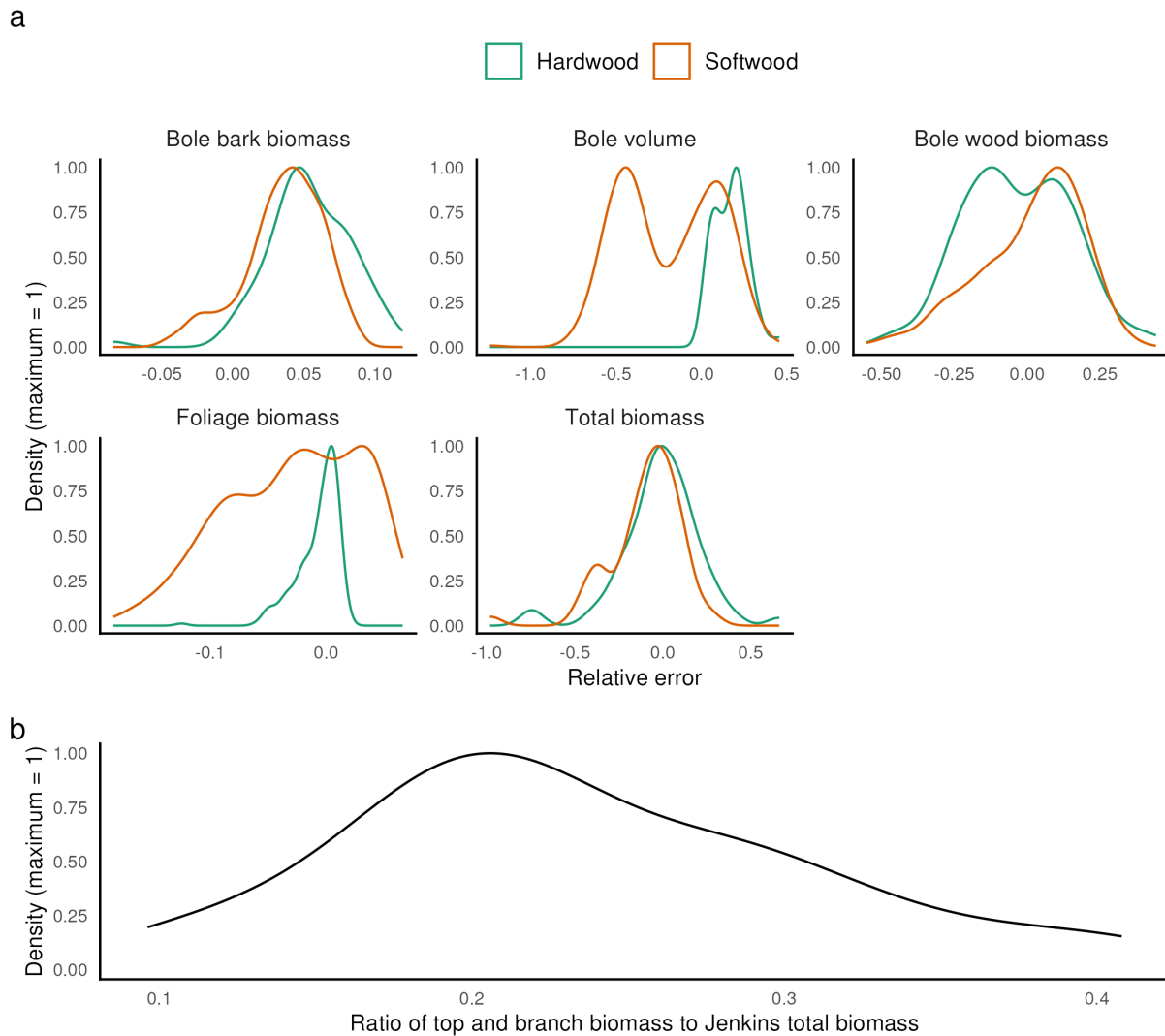


Figure B1: Smoothed frequency distributions of allometric model uncertainty information compiled from the legacy tree database. Distributions for all individual panels have been rescaled separately, such that the most common occurrences within each panel are assigned a value of 1. a) Relative residuals for five estimated tree components. Bole volume residuals are relative to bole volume, while all biomass residuals are relative to total tree biomass. b) Ratios for top and branch biomass relative to total biomass.



**Appendix C: Reference data uncertainty**

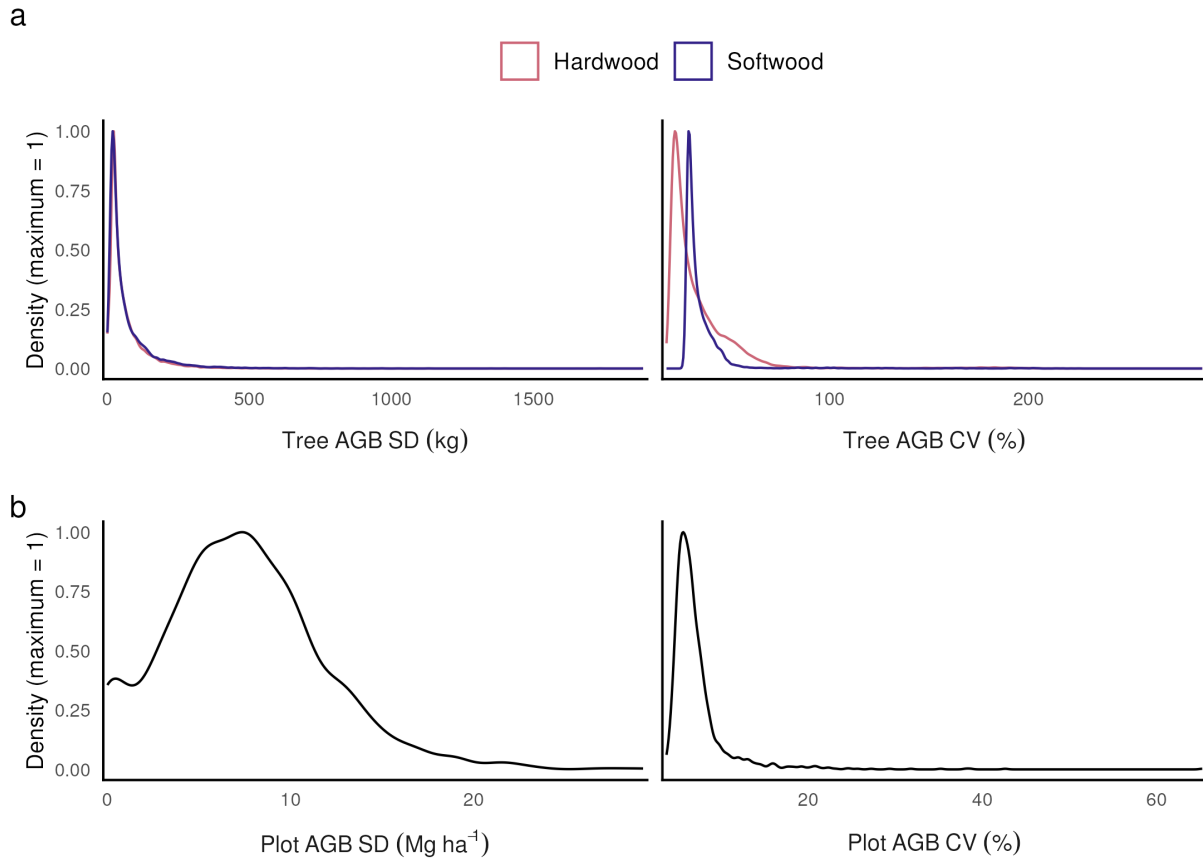


Figure C1: Reference data uncertainty. Smoothed frequency distributions estimates for individual tree (a) and plot (b) AGB standard deviations (SD) and coefficients of variation (CV;  $SD/AGB \cdot 100$ ) over the 1000 bootstrap iterations. Distributions for individual panels have been rescaled separately such that the most common occurrences within each panel are assigned a value of 1.

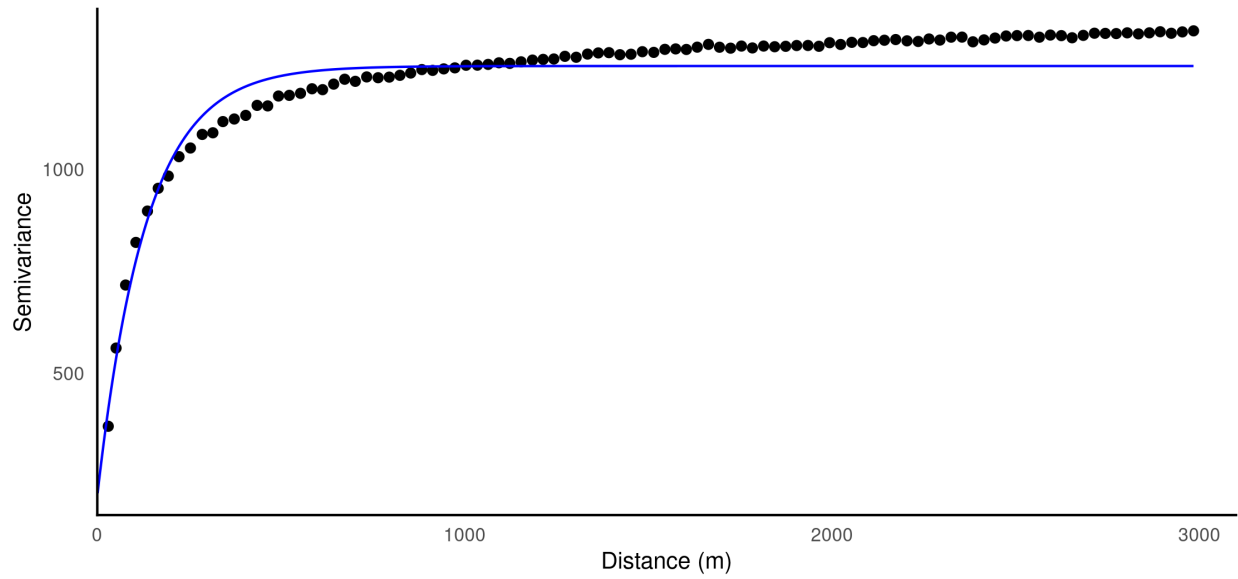
**Appendix D: Spatial autocorrelation of residuals**

Figure D1: Exponential model semivariogram (blue line) fit to empirical semivariogram (black points) computed with a simple random spatial sample of 500,000 residuals (linear scale). Refer to equation 11 in the main body of the text for residual definition.

**Appendix E: Residual variance model**

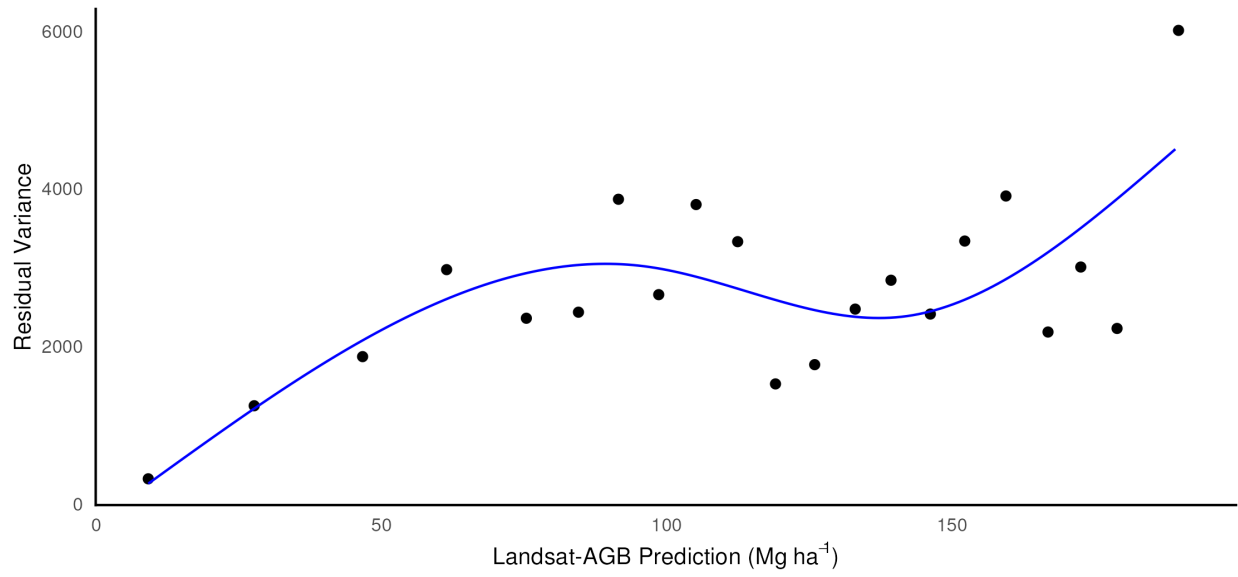


Figure E1: Natural cubic spline residual variance model fit (blue line) representing residual variance as a function of AGB prediction.

## Appendix F: Modeling estimated standard error (total variance) as a function of parcel characteristics

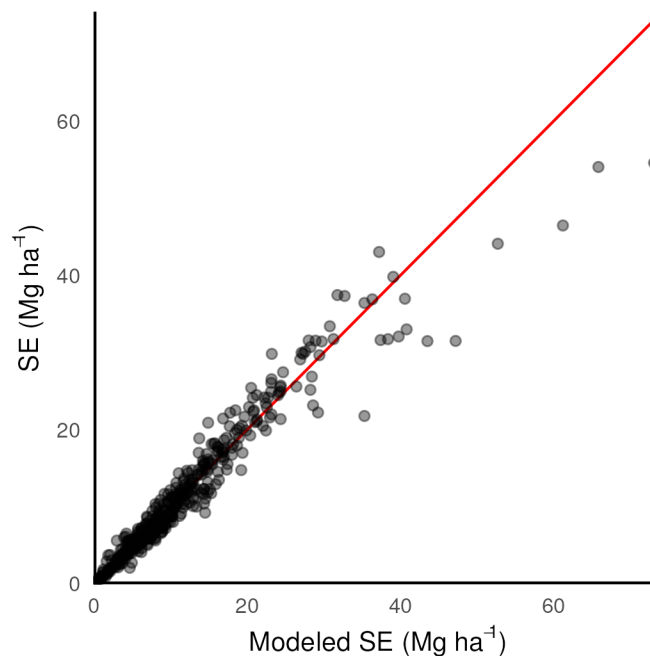


Figure F1: Standard error (SE) estimated with Equations 1 and 2 vs SE estimated from a natural log-log regression with parcel area, perimeter, AGB density, and % forest cover as independent variables. Each point represents a parcel from the testing partition of the sample. 1:1 line in red.

## References

- Baskerville, G. L. 1972. "Use of Logarithmic Regression in the Estimation of Plant Biomass." *Canadian Journal of Forest Research* 2 (1): 49–53. <https://doi.org/10.1139/x72-009>.
- Baston, Daniel. 2022. *Exactextractr: Fast Extraction from Raster Datasets Using Polygons*. <https://CRAN.R-project.org/package=exactextractr>.
- Bechtold, William A, and Paul L Patterson. 2005. *The Enhanced Forest Inventory and Analysis Program—National Sampling Design and Estimation Procedures*. Vol. 80. USDA Forest Service, Southern Research Station. <https://doi.org/10.2737/SRS-GTR-80>.
- Berger, Ambros, Thomas Gschwantner, Ronald E. McRoberts, and Klemens Schadauer. 2014. "Effects of Measurement Errors on Individual Tree Stem Volume Estimates for the Austrian National Forest Inventory." *Forest Science* 60 (1): 14–24. <https://doi.org/10.5849/forsci.12-164>.
- Breidenbach, Johannes, Clara Antón-Fernández, Hans Petersson, Ronald E. McRoberts, and Rasmus Astrup. 2014. "Quantifying the Model-Related Variability of Biomass Stock and Change Estimates in the Norwegian National Forest Inventory." *Forest Science* 60 (1): 25–33. <https://doi.org/10.5849/forsci.12-137>.
- Breidenbach, Johannes, Ronald E. McRoberts, and Rasmus Astrup. 2016. "Empirical Coverage of Model-Based Variance Estimators for Remote Sensing Assisted Estimation of Stand-Level Timber Volume." *Remote Sensing of Environment* 173 (February): 274–81. <https://doi.org/10.1016/j.rse.2015.07.026>.
- Breiman, Leo. 2001a. "Random Forests." *Machine Learning* 45 (1): 5–32. <https://doi.org/10.1023/A:1010933404324>.
- . 2001b. "Statistical Modeling: The Two Cultures (with Comments and a Rejoinder by the Author)." *Statistical Science* 16 (3). <https://doi.org/10.1214/ss/1009213726>.
- Brown, Jesslyn F., Heather J. Tollerud, Christopher P. Barber, Qiang Zhou, John L. Dwyer, James E. Vogelmann, Thomas R. Loveland, et al. 2020. "Lessons learned implementing an operational continuous United States national land change monitoring capability: The Land Change Monitoring, Assessment, and Projection (LCMAP) approach." *Remote Sensing of Environment* 238: 111356. <https://doi.org/10.1016/j.rse.2019.111356>.
- Buendia, E, K Tanabe, A Kranjc, J Baasansuren, M Fukuda, S Ngarize, A Osako, Y Pyrozhenko, P Shermanau, and S Federici. 2019. "Refinement to the 2006 IPCC Guidelines for National Greenhouse Gas Inventories." *IPCC: Geneva, Switzerland* 5: 194.

- Butler, Brett J., Jaketon H. Hewes, Brenton J. Dickinson, Kyle Andrejczyk, Sarah M. Butler, and Marla Markowski-Lindsay. 2016. "Family Forest Ownerships of the United States, 2013: Findings from the USDA Forest Service's National Woodland Owner Survey." *Journal of Forestry* 114 (6): 638–47. <https://doi.org/10.5849/jof.15-099>.
- CEOS. 2021. "Aboveground Woody Biomass Product Validation Good Practices Protocol." <https://doi.org/10.5067/DO/CEOSWGCV/LPV/AGB.001>.
- Chave, Jérôme, Maxime Réjou-Méchain, Alberto Búrquez, Emmanuel Chidumayo, Matthew S. Colgan, Wellington B. C. Delitti, Alvaro Duque, et al. 2014. "Improved Allometric Models to Estimate the Aboveground Biomass of Tropical Trees." *Global Change Biology* 20 (10): 3177–90. <https://doi.org/10.1111/gcb.12629>.
- Chen, Qi, Gaia Vaglio Laurin, and Riccardo Valentini. 2015. "Uncertainty of Remotely Sensed Aboveground Biomass over an African Tropical Forest: Propagating Errors from Trees to Plots to Pixels." *Remote Sensing of Environment* 160 (April): 134–43. <https://doi.org/10.1016/j.rse.2015.01.009>.
- Chen, Qi, Ronald E. McRoberts, Changwei Wang, and Philip J. Radtke. 2016. "Forest Aboveground Biomass Mapping and Estimation Across Multiple Spatial Scales Using Model-Based Inference." *Remote Sensing of Environment* 184 (October): 350–60. <https://doi.org/10.1016/j.rse.2016.07.023>.
- Cooke, William H. 2000. "Forest/Non-Forest Stratification in Georgia with Landsat Thematic Mapper Data." In *McRoberts, Ronald e.; Reams, Gregory a.; van Deusen, Paul c., Eds. Proceedings of the First Annual Forest Inventory and Analysis Symposium; Gen. Tech. Rep. NC-213. St. Paul, MN: US Department of Agriculture, Forest Service, North Central Research Station: 28-30.*
- Cortes, Corinna, and Vladimir Vapnik. 1995. "Support-Vector Networks." *Machine Learning* 20 (3): 273–97. <https://doi.org/10.1007/bf00994018>.
- Domke, Grant M, Christopher W Woodall, and James E Smith. 2011. "Accounting for Density Reduction and Structural Loss in Standing Dead Trees: Implications for Forest Biomass and Carbon Stock Estimates in the United States." *Carbon Balance and Management* 6 (1). <https://doi.org/10.1186/1750-0680-6-14>.
- Dubayah, Ralph, James Bryan Blair, Scott Goetz, Lola Fatoyinbo, Matthew Hansen, Sean Healey, Michelle Hofton, et al. 2020. "The Global Ecosystem Dynamics Investigation: High-Resolution Laser Ranging of the Earth's Forests and Topography." *Science of Remote Sensing* 1 (June): 100002. <https://doi.org/10.1016/j.srs.2020.100002>.
- Dyer, James M. 2006. "Revisiting the Deciduous Forests of Eastern North America." *BioScience* 56 (4): 341–52. [https://doi.org/10.1641/0006-3568\(2006\)56%5B341:RTDFOE%5D2.0.CO;2](https://doi.org/10.1641/0006-3568(2006)56%5B341:RTDFOE%5D2.0.CO;2).
- Earth Resources Observation And Science (EROS) Center. 2019. "National Agriculture Imagery Program (NAIP)." U.S. Geological Survey. <https://doi.org/10.5066/F7QN651G>.
- Efron, Bradley. 2020. "Prediction, Estimation, and Attribution." *Journal of the American Statistical Association* 115 (530): 636–55. <https://doi.org/10.1080/01621459.2020.1762613>.
- Efron, Bradley, and Robert J Tibshirani. 1994. *An Introduction to the Bootstrap*. CRC press.
- Eggleston, H S, L Buendia, K Miwa, T Ngara, and K Tanabe. 2006. "2006 IPCC Guidelines for National Greenhouse Gas Inventories."
- Esteban, Jessica, Ronald E. McRoberts, Alfredo Fernández-Landa, José Luis Tomé, and Miguel Marchamalo. 2020. "A Model-Based Volume Estimator That Accounts for Both Land Cover Misclassification and Model Prediction Uncertainty." *Remote Sensing* 12 (20): 3360. <https://doi.org/10.3390/rs12203360>.
- Freedman, David A. 1981. "Bootstrapping Regression Models." *The Annals of Statistics* 9 (6): 1218–28. <https://doi.org/10.1214/aos/1176345638>.
- Friedman, Jerome H. 2002. "Stochastic Gradient Boosting." *Computational Statistics and Data Analysis* 38 (4): 367–78. [https://doi.org/10.1016/S0167-9473\(01\)00065-2](https://doi.org/10.1016/S0167-9473(01)00065-2).
- Gräler, Benedikt, Edzer Pebesma, and Gerard Heuvelink. 2016. "Spatio-Temporal Interpolation using gstat." *The R Journal* 8 (1): 204–18. <https://doi.org/10.32614/RJ-2016-014>.
- Gray, Andrew N, Thomas J Brandeis, John D Shaw, William H McWilliams, and Patrick Miles. 2012. "Forest Inventory and Analysis Database of the United States of America (FIA)." *Biodiversity and Ecology* 4: 225–31. <https://doi.org/10.7809/b-e.00079>.
- Harmon, Mark E., Christopher W. Woodall, Becky Fasth, Jay Sexton, and Misha. Yatkov. 2011. *Differences Between Standing and Downed Dead Tree Wood Density Reduction Factors: A Comparison Across Decay Classes and Tree Species*. U.S. Department of Agriculture, Forest Service, Northern Research Station. <https://doi.org/10.2737/nrs-rp-15>.
- Hastie, Trevor J. 1992. "Generalized Additive Models." In *Chapter 7 of Statistical Models in s*, edited by DM Bates, JM Chambers, and T Hastie. Routledge.
- Hijmans, Robert J. 2023. *Terra: Spatial Data Analysis*. <https://CRAN.R-project.org/package=terra>.
- Hoppus, Michael, and Andrew Lister. 2005. "The Status of Accurately Locating Forest Inventory and Analysis Plots Using the Global Positioning System." In *Proceedings of the Seventh Annual Forest Inventory and Analysis Symposium*. <https://www.fs.usda.gov/research/treesearch/17040>.
- Huang, Wenli, Katelyn Dolan, Anu Swatantran, Kristofer Johnson, Hao Tang, Jarlath O'Neil-Dunne, Ralph Dubayah, and George Hurtt. 2019. "High-resolution mapping of aboveground biomass for forest carbon monitoring system

- in the Tri-State region of Maryland, Pennsylvania and Delaware, USA.” *Environmental Research Letters* 14 (9): 095002. <https://doi.org/10.1088/1748-9326/ab2917>.
- Hudak, Andrew T, Patrick A Fekety, Van R Kane, Robert E Kennedy, Steven K Filippelli, Michael J Falkowski, Wade T Tinkham, et al. 2020. “A Carbon Monitoring System for Mapping Regional, Annual Aboveground Biomass Across the Northwestern USA.” *Environmental Research Letters* 15 (9): 095003. <https://doi.org/10.1088/1748-9326/ab93f9>.
- Jenkins, Jennifer C, David C Chojnacky, Linda S Heath, and Richard A Birdsey. 2003. “National-Scale Biomass Estimators for United States Tree Species.” *Forest Science* 49 (1): 12–35. <https://academic.oup.com/forestscience/article/49/1/12/4617214>.
- Johnson, Kristofer D., Richard Birdsey, Jason Cole, Anu Swatantran, Jarlath O’Neil-Dunne, Ralph Dubayah, and Andrew Lister. 2015. “Integrating LIDAR and Forest Inventories to Fill the Trees Outside Forests Data Gap.” *Environmental Monitoring and Assessment* 187 (10). <https://doi.org/10.1007/s10661-015-4839-1>.
- Johnson, Lucas K., Michael J. Mahoney, Eddie Bevilacqua, Stephen V. Stehman, Grant M. Domke, and Colin M. Beier. 2022. “Fine-Resolution Landscape-Scale Biomass Mapping Using a Spatiotemporal Patchwork of LiDAR Coverages.” *International Journal of Applied Earth Observation and Geoinformation* 114 (November): 103059. <https://doi.org/10.1016/j.jag.2022.103059>.
- Johnson, Lucas K., Michael J. Mahoney, Madeleine L. Desrochers, and Colin M. Beier. 2023. “Mapping Historical Forest Biomass for Stock-Change Assessments at Parcel to Landscape Scales.” *Forest Ecology and Management* 546 (October): 121348. <https://doi.org/10.1016/j.foreco.2023.121348>.
- Karatzoglou, Alexandros, Alex Smola, Kurt Hornik, and Achim Zeileis. 2004. “Kernlab – an S4 Package for Kernel Methods in R.” *Journal of Statistical Software* 11 (9): 1–20. <https://doi.org/10.18637/jss.v011.i09>.
- Kattenborn, Teja, Jens Leitloff, Felix Schiefer, and Stefan Hinz. 2021. “Review on Convolutional Neural Networks (CNN) in Vegetation Remote Sensing.” *ISPRS Journal of Photogrammetry and Remote Sensing* 173 (March): 24–49. <https://doi.org/10.1016/j.isprsjprs.2020.12.010>.
- Ke, Guolin, Qi Meng, Thomas Finley, Taifeng Wang, Wei Chen, Weidong Ma, Qiwei Ye, and Tie-Yan Liu. 2017. “LightGBM: A Highly Efficient Gradient Boosting Decision Tree.” In *Advances in Neural Information Processing Systems*, edited by I. Guyon, U. V. Luxburg, S. Bengio, H. Wallach, R. Fergus, S. Vishwanathan, and R. Garnett. Vol. 30. Curran Associates, Inc. <https://proceedings.neurips.cc/paper/2017/file/6449f44a102fde848669bdd9eb6b76fa-Paper.pdf>.
- Kennedy, Robert E, Janet Ohmann, Matt Gregory, Heather Roberts, Zhiqiang Yang, David M Bell, Van Kane, et al. 2018. “An Empirical, Integrated Forest Biomass Monitoring System.” *Environmental Research Letters* 13 (2): 025004. <https://doi.org/10.1088/1748-9326/aa9d9e>.
- Kennedy, Robert E, Zhiqiang Yang, and Warren B. Cohen. 2010. “Detecting Trends in Forest Disturbance and Recovery Using Yearly Landsat Time Series: 1. LandTrendr — Temporal Segmentation Algorithms.” *Remote Sensing of Environment* 114 (12): 2897–2910. <https://doi.org/10.1016/j.rse.2010.07.008>.
- Kennedy, Robert E, Zhiqiang Yang, Noel Gorelick, Justin Braaten, Lucas Cavalcante, Warren B. Cohen, and Sean Healey. 2018. “Implementation of the LandTrendr Algorithm on Google Earth Engine.” *Remote Sensing* 10 (5). <https://doi.org/10.3390/rs10050691>.
- Knapp, Alan K., John M. Briggs, Scott L. Collins, Steven R. Arecher, M. Syndonia Bret-Harte, Brent E. Ewers, Debra P. Peters, et al. 2007. “Shrub Encroachment in North American Grasslands: Shifts in Growth Form Dominance Rapidly Alters Control of Ecosystem Carbon Inputs.” *Global Change Biology* 14 (3): 615–23. <https://doi.org/10.1111/j.1365-2486.2007.01512.x>.
- Kuhn, Max, Davis Vaughan, and Emil Hvitfeldt. 2023. *Yardstick: Tidy Characterizations of Model Performance*. <https://CRAN.R-project.org/package=yardstick>.
- “Kyoto Protocol to the United Nations Framework Convention on Climate Change.” 1997. UN Treaty. <https://treaties.un.org/doc/Publication/UNTS/Volume%202303/v2303.pdf>.
- L’Roe, Andrew W, and Shorna Broussard Allred. 2013. “Thriving or Surviving? Forester Responses to Private Forestland Parcelization in New York State.” *Small-Scale Forestry* 12 (3): 353–76. <https://doi.org/10.1007/s11842-012-9216-0>.
- Labrière, Nicolas, Stuart J. Davies, Mathias I. Disney, Laura I. Duncanson, Martin Herold, Simon L. Lewis, Oliver L. Phillips, et al. 2022. “Toward a Forest Biomass Reference Measurement System for Remote Sensing Applications.” *Global Change Biology* 29 (3): 827–40. <https://doi.org/10.1111/gcb.16497>.
- Landau, William Michael. 2021. “The Targets r Package: A Dynamic Make-Like Function-Oriented Pipeline Toolkit for Reproducibility and High-Performance Computing.” *Journal of Open Source Software* 6 (57): 2959. <https://doi.org/10.21105/joss.02959>.
- LeCun, Yann, Yoshua Bengio, and Geoffrey Hinton. 2015. “Deep Learning.” *Nature* 521 (7553): 436–44. <https://doi.org/10.1038/nature14539>.
- Liu, Regina Y. 1988. “Bootstrap Procedures Under Some Non-i.i.d. Models.” *The Annals of Statistics* 16 (4). <https://doi.org/10.1214/aos/1176351062>.

- Liu, Siyu, Martin Brandt, Thomas Nord-Larsen, Jerome Chave, Florian Reiner, Nico Lang, Xiaoye Tong, et al. 2023. “The Overlooked Contribution of Trees Outside Forests to Tree Cover and Woody Biomass Across Europe.” *Science Advances* 9 (37). <https://doi.org/10.1126/sciadv.adh4097>.
- Mahoney, Michael J, Lucas K Johnson, Abigail Z Guinan, and Colin M Beier. 2022. “Classification and Mapping of Low-Statured Shrubland Cover Types in Post-Agricultural Landscapes of the US Northeast.” *International Journal of Remote Sensing* 43 (19–24): 7117–38. <https://doi.org/10.1080/01431161.2022.2155086>.
- Matasci, Giona, Txomin Hermosilla, Michael A. Wulder, Joanne C. White, Nicholas C. Coops, Geordie W. Hobart, Douglas K. Bolton, Piotr Tompalski, and Christopher W. Bater. 2018. “Three Decades of Forest Structural Dynamics over Canada's Forested Ecosystems Using Landsat Time-Series and Lidar Plots.” *Remote Sensing of Environment* 216 (October): 697–714. <https://doi.org/10.1016/j.rse.2018.07.024>.
- McRoberts, Ronald E. 2011. “Satellite Image-Based Maps: Scientific Inference or Pretty Pictures?” *Remote Sensing of Environment* 115 (2): 715–24. <https://doi.org/10.1016/j.rse.2010.10.013>.
- McRoberts, Ronald E., Qi Chen, Grant M. Domke, Göran Ståhl, Svetlana Saarela, and James A. Westfall. 2016. “Hybrid Estimators for Mean Aboveground Carbon Per Unit Area.” *Forest Ecology and Management* 378 (October): 44–56. <https://doi.org/10.1016/j.foreco.2016.07.007>.
- McRoberts, Ronald E., Erik Næsset, Terje Gobakken, Gherardo Chirici, Sonia Condés, Zhengyang Hou, Svetlana Saarela, Qi Chen, Göran Ståhl, and Brian F. Walters. 2018. “Assessing Components of the Model-Based Mean Square Error Estimator for Remote Sensing Assisted Forest Applications.” *Canadian Journal of Forest Research* 48 (6): 642–49. <https://doi.org/10.1139/cjfr-2017-0396>.
- McRoberts, Ronald E., Erik Næsset, Zhengyang Hou, Göran Ståhl, Svetlana Saarela, Jessica Esteban, Davide Travaglini, Jahangir Mohammadi, and Gherardo Chirici. 2023. “How Many Bootstrap Replications Are Necessary for Estimating Remote Sensing-Assisted, Model-Based Standard Errors?” *Remote Sensing of Environment* 288 (April): 113455. <https://doi.org/10.1016/j.rse.2023.113455>.
- McRoberts, Ronald E., Erik Næsset, Sassan Saatchi, and Shaun Quegan. 2022. “Statistically Rigorous, Model-Based Inferences from Maps.” *Remote Sensing of Environment* 279 (September): 113028. <https://doi.org/10.1016/j.rse.2022.113028>.
- McRoberts, Ronald E., Erkki O. Tomppo, and Erik Næsset. 2010. “Advances and Emerging Issues in National Forest Inventories.” *Scandinavian Journal of Forest Research* 25 (4): 368–81. <https://doi.org/10.1080/02827581.2010.496739>.
- McRoberts, Ronald E., and James A. Westfall. 2014. “Effects of Uncertainty in Model Predictions of Individual Tree Volume on Large Area Volume Estimates.” *Forest Science* 60 (1): 34–42. <https://doi.org/10.5849/forsci.12-141>.
- Meyer, Hanna, and Edzer Pebesma. 2021. “Predicting into unknown space? Estimating the area of applicability of spatial prediction models.” *Methods in Ecology and Evolution* 12 (9): 1620–33. <https://doi.org/10.1111/2041-210x.13650>.
- Nelson, Mark D., Greg C. Liknes, and Brett J. Butler. 2010. *Map of Forest Ownership in the Conterminous United States. [Scale 1:7, 500, 000]*. U.S. Department of Agriculture, Forest Service, Northern Research Station. <https://doi.org/10.2737/nrs-rmap-2>.
- Pan, Yude, Richard A. Birdsey, Jingyun Fang, Richard Houghton, Pekka E. Kauppi, Werner A. Kurz, Oliver L. Phillips, et al. 2011. “A Large and Persistent Carbon Sink in the World's Forests.” *Science* 333 (6045): 988–93. <https://doi.org/10.1126/science.1201609>.
- “Paris Agreement to the United Nations Framework Convention on Climate Change.” 2015. UN Treaty. United Nations. <https://treaties.un.org/doc/Publication/UNTS/Volume%203156/Part/volume-3156-I-54113.pdf>.
- Pebesma, Edzer J. 2004. “Multivariable Geostatistics in s: The Gstat Package.” *Computers & Geosciences* 30 (7): 683–91. <https://doi.org/10.1016/j.cageo.2004.03.012>.
- Penman, J., M. Gytarski, T. Hiraishi, T. Krug, D. Kruger, R. Pipatti, L. Buendia, et al. 2003. “Good Practice Guidance for Land Use, Land-Use Change and Forestry.” <http://www.ipcc-nggip.iges.or.jp/public/gpglulucf/gpglulucf.htm>.
- Perry, Charles H, Mark V Finco, T Barry, et al. 2022. “Forest Atlas of the United States.” *FS-1172* 1172.
- Quegan, Shaun, Thuy Le Toan, Jerome Chave, Jorgen Dall, Jean-François Exbrayat, Dinh Ho Tong Minh, Mark Lomas, et al. 2019. “The European Space Agency BIOMASS Mission: Measuring Forest Above-Ground Biomass from Space.” *Remote Sensing of Environment* 227 (June): 44–60. <https://doi.org/10.1016/j.rse.2019.03.032>.
- R Core Team. 2023. *R: A Language and Environment for Statistical Computing*. Vienna, Austria: R Foundation for Statistical Computing. <https://www.R-project.org/>.
- Radtke, PJ, DM Walker, AR Weiskittel, J Frank, JW Coulston, and JA Westfall. 2015. “Legacy Tree Data: A National Database of Detailed Tree Measurements for Volume, Weight, and Physical Properties.” In *Pushing Boundaries: New Directions in Inventory Techniques and Applications: Forest Inventory and Analysis (FIA) Symposium*, 2015:8–10. <https://www.fs.usda.gov/research/treesearch/50166>.
- Raile, Gerhard K. 1982. “Estimating Stump Volume.” U.S. Department of Agriculture, Forest Service, North Central Forest Experiment Station. <https://doi.org/10.2737/nc-rp-224>.
- Rogers, Paul. 1996. “Disturbance Ecology and Forest Management: A Review of the Literature.” [https://www.fs.usda.gov/rm/pubs\\_int/int\\_gtr336.pdf](https://www.fs.usda.gov/rm/pubs_int/int_gtr336.pdf).

- Ross, Robert J. 2021. “Wood Handbook: Wood as an Engineering Material.” <https://www.fs.usda.gov/research/treesearch/62200>.
- Saarela, Svetlana, Sören Holm, Anton Grafström, Sebastian Schnell, Erik Næsset, Timothy G. Gregoire, Ross F. Nelson, and Göran Ståhl. 2016. “Hierarchical Model-Based Inference for Forest Inventory Utilizing Three Sources of Information.” *Annals of Forest Science* 73 (4): 895–910. <https://doi.org/10.1007/s13595-016-0590-1>.
- Saarela, Svetlana, Sören Holm, Sean Healey, Hans-Erik Andersen, Hans Petersson, Wilmer Prentius, Paul Patterson, Erik Næsset, Timothy Gregoire, and Göran Ståhl. 2018. “Generalized Hierarchical Model-Based Estimation for Aboveground Biomass Assessment Using GEDI and Landsat Data.” *Remote Sensing* 10 (11): 1832. <https://doi.org/10.3390/rs10111832>.
- Saarela, Svetlana, André Wästlund, Emma Holmström, Alex Appiah Mensah, Sören Holm, Mats Nilsson, Jonas Fridman, and Göran Ståhl. 2020. “Mapping Aboveground Biomass and Its Prediction Uncertainty Using LiDAR and Field Data, Accounting for Tree-Level Allometric and LiDAR Model Errors.” *Forest Ecosystems* 7 (1). <https://doi.org/10.1186/s40663-020-00245-0>.
- Schnell, Sebastian, Dan Altrell, Göran Ståhl, and Christoph Kleinn. 2014. “The Contribution of Trees Outside Forests to National Tree Biomass and Carbon Stocks—A Comparative Study Across Three Continents.” *Environmental Monitoring and Assessment* 187 (1). <https://doi.org/10.1007/s10661-014-4197-4>.
- Schoeneberger, Michele M. 2009. “Agroforestry: Working Trees for Sequestering Carbon on Agricultural Lands.” *Agroforestry Systems* 75: 27–37. <https://doi.org/10.1007/s10457-008-9123-8>.
- Scott, Charles Thomas. 1981. *Northeastern Forest Survey Revised Cubic-Foot Volume Equations*. Vol. 304. US Department of Agriculture, Forest Service, Northeastern Forest Experiment . . . [https://www.fs.usda.gov/ne/newton\\_square/publications/research\\_notes/pdfs/scanned/OCR/ne\\_rn304.pdf](https://www.fs.usda.gov/ne/newton_square/publications/research_notes/pdfs/scanned/OCR/ne_rn304.pdf).
- Seymour, Robert S, Alan S White, and Philip G deMaynadier. 2002. “Natural Disturbance Regimes in Northeastern North America—Evaluating Silvicultural Systems Using Natural Scales and Frequencies.” *Forest Ecology and Management* 155 (1–3): 357–67. [https://doi.org/10.1016/s0378-1127\(01\)00572-2](https://doi.org/10.1016/s0378-1127(01)00572-2).
- Shi, Yu, Guolin Ke, Damien Soukhavong, James Lamb, Qi Meng, Thomas Finley, Taifeng Wang, et al. 2022. *Lightgbm: Light Gradient Boosting Machine*. <https://github.com/Microsoft/LightGBM>.
- Sprugel, D. G. 1983. “Correcting for Bias in Log-transformed Allometric Equations.” *Ecology* 64 (1): 209–10. <https://doi.org/10.2307/1937343>.
- Ståhl, Göran, Juha Heikkinen, Hans Petersson, Jaakko Repola, and Sören Holm. 2014. “Sample-Based Estimation of Greenhouse Gas Emissions from Forests—A New Approach to Account for Both Sampling and Model Errors.” *Forest Science* 60 (1): 3–13. <https://doi.org/10.5849/forsci.13-005>.
- Stehman, Stephen V., Bruce W. Pengra, Josephine A. Horton, and Danika F. Wellington. 2021. “Validation of the u.s. Geological Survey’s Land Change Monitoring, Assessment and Projection (LCMAP) Collection 1.0 Annual Land Cover Products 1985–2017.” *Remote Sensing of Environment* 265 (November): 112646. <https://doi.org/10.1016/j.rse.2021.112646>.
- “The United Nations Framework Convention on Climate Change.” 1992. UN Treaty. <https://treaties.un.org/doc/Publication/UNTS/Volume%201771/v1771.pdf>.
- Udawatta, Ranjith P., and Shibu Jose. 2011. “Carbon Sequestration Potential of Agroforestry Practices in Temperate North America.” In *Carbon Sequestration Potential of Agroforestry Systems*, 17–42. Springer Netherlands. [https://doi.org/10.1007/978-94-007-1630-8\\_2](https://doi.org/10.1007/978-94-007-1630-8_2).
- USDA Forest Service. 2020. “Forests of New York, 2019.” U.S. Department of Agriculture, Forest Service, Northern Research Station. <https://doi.org/10.2737/fs-ru-250>.
- USFS. 2020. “Forests of New York, 2019.” United States Department of Agriculture, Forest Service; U.S. Department of Agriculture, Forest Service, Northern Research Station. <https://doi.org/10.2737/fs-ru-250>.
- Van Auken, O. W. 2000. “Shrub Invasions of North American Semiarid Grasslands.” *Annual Review of Ecology and Systematics* 31 (1): 197–215. <https://doi.org/10.1146/annurev.ecolsys.31.1.197>.
- Wadoux, Alexandre M. J.-C., and Gerard B. M. Heuvelink. 2023. “Uncertainty of Spatial Averages and Totals of Natural Resource Maps.” *Methods in Ecology and Evolution* 14 (5): 1320–32. <https://doi.org/10.1111/2041-210x.14106>.
- Webster, Richard, and Margaret A Oliver. 2007. *Geostatistics for Environmental Scientists*. John Wiley & Sons.
- Westfall, James A., John W. Coulston, Andrew N. Gray, John D. Shaw, Philip J. Radtke, David M. Walker, Aaron R. Weiskittel, et al. 2023. “A National-Scale Tree Volume, Biomass, and Carbon Modeling System for the United States.” U.S. Department of Agriculture, Forest Service. <https://doi.org/10.2737/wo-gtr-104>.
- Woodall, Christopher W., John W. Coulston, Grant M. Domke, Brian F. Walters, David N. Wear, James E. Smith, Hans-Erik Andersen, et al. 2015. “The u.s. Forest Carbon Accounting Framework: Stocks and Stock Change, 1990-2016.” U.S. Department of Agriculture, Forest Service, Northern Research Station. <https://doi.org/10.2737/nrs-gtr-154>.
- Woodall, Christopher W., Linda S. Heath, Grant M. Domke, and Michael C. Nichols. 2011. “Methods and Equations for Estimating Aboveground Volume, Biomass, and Carbon for Trees in the u.s. Forest Inventory, 2010.” U.S. Department of Agriculture, Forest Service, Northern Research Station. <https://doi.org/10.2737/nrs-gtr-88>.



- Wright, Marvin N., and Andreas Ziegler. 2017. "ranger: A Fast Implementation of Random Forests for High Dimensional Data in C++ and R." *Journal of Statistical Software* 77 (1): 1–17. <https://doi.org/10.18637/jss.v077.i01>.
- Yanai, Ruth D., Alexander R. Young, John L. Campbell, James A. Westfall, Charles J. Barnett, Gretchen A. Dillon, Mark B. Green, and Christopher W. Woodall. 2023. "Measurement Uncertainty in a National Forest Inventory: Results from the Northern Region of the USA." *Canadian Journal of Forest Research* 53 (3): 163–77. <https://doi.org/10.1139/cjfr-2022-0062>.
- Zhu, Zhe, and Curtis E. Woodcock. 2014. "Continuous change detection and classification of land cover using all available Landsat data." *Remote Sensing of Environment* 144: 152–71. <https://doi.org/10.1016/j.rse.2014.01.011>.